Title: CDC20B is required for deuterosome-mediated centriole production in multiciliated cells

Authors: Diego R. Revinski[1†], Laure-Emmanuelle Zaragosi[2†], Camille Boutin[1†], Sandra Ruiz-Garcia[2], Marie Deprez[2], Olivier Rosnet[1], Virginie Thomé[1], Olivier Mercey[2], Agnès Paquet[2], Nicolas Pons[2], Brice Marcet[2*], Laurent Kodjabachian[1*], Pascal Barbry[2*]

Affiliations:

[1] Aix Marseille Univ, CNRS, IBDM, Marseille, France

[2] Université Côte d'Azur, CNRS, IPMC, Sophia-Antipolis, France.

[†] These authors contributed equally

[*]Correspondence to: marcet@ipmc.cnrs.fr; laurent.kodjabachian@univ-amu.fr; barbry@ipmc.cnrs.fr

Keywords: multiciliated cell, centriole, deuterosome, CDC20B, separase, cell cycle, *Xenopus*, mouse, human

Introductory paragraph: Multiciliated cells (MCCs) harbour dozens to hundreds of motile cilia, which beat in a synchronized and directional manner, thus generating hydrodynamic forces important in animal physiology[1, 2]. In vertebrates, MCC differentiation critically depends on the synthesis and release of numerous centrioles by specialized structures called deuterosomes[1-5]. Little is known about the composition, organization and regulation of deuterosomes. Here, single-cell RNA sequencing reveals that human deuterosome-stage MCCs are characterized by the expression of many cell cycle-related genes. Among those, we further investigated the uncharacterized vertebrate-specific *cell division cycle 20B* (*CDC20B*) gene. We show that the CDC20B protein associates to the deuterosome, and is required for the production of centrioles and cilia in mouse and *Xenopus* MCCs. In *Xenopus*, centrioles and cilia were efficiently rescued in absence of CDC20B by over-expression of the protease Separase, linking CDC20B function to centriole release from deuterosomes, in analogy to centriole disengagement in mitotic cells. This work reveals the shaping of a new biological function, deuterosome-mediated centriole production in vertebrate MCCs, by adaptation between ancestral and recently evolved cell cycle-related molecules.

Main text: Multiciliated cells (MCCs) are present throughout metazoan evolution and serve functions ranging from locomotion of marine larvae and flatworms, to brain homeostasis, mucociliary clearance of pathogens and transportation of oocytes in vertebrates[1, 2, 6]. The formation of MCCs requires the production of numerous motile cilia through a complex process called multiciliogenesis[1, 2]. Recently, defective multiciliogenesis has been associated with human congenital respiratory and fertility syndromes[7, 8]. Each cilium sits atop a modified centriole, called a basal body (BB). After they exit from the cell cycle, maturing MCCs face the challenge of producing hundreds of centrioles in a limited time window. In vertebrate MCCs, bulk centriole biogenesis is mostly achieved through an acentriolar structure named

the deuterosome, although canonical amplification from parental centrioles also occurs[1, 2, 6]. Recent studies have suggested that deuterosome-mediated centriole synthesis mobilizes proteins usually involved in the centriole-dependent duplication pathway of the cell cycle, such as PLK4, CEP152 and SAS6[3-5]. However, the deuterosome pathway also mobilizes specific components, structurally related to cell cycle molecules, such as the Geminin-related protein Multicilin (MCIDAS in mammals), which is necessary and sufficient to drive multiciliogenesis[9], or the CEP63 paralogue DEUP1, an essential component of deuterosome assembly[5]. To better understand deuterosome biology, we used single-cell RNA sequencing (scRNA-seq) to identify genes expressed in maturing MCCs during the phase of centriole amplification.

We applied scRNA-seq analyses to 3D air-liquid primary cultures of human airway epithelial cells (HAECs) at the differentiation stage corresponding to active centriole multiplication[10] (Fig. 1a). Gene expression data from 1663 cells was projected on a 2D space by *t*-distributed Stochastic Neighbor Embedding (tSNE) (Fig. 1b). We identified a small group of 37 cells corresponding to maturing MCCs engaged in deuterosome-mediated centriole amplification, as revealed by the specific expression of *MCIDAS*[9], *MYB*[11], and *DEUP1*[5] (Fig. 1c,d and Supplementary Fig. 1). This subpopulation was characterized by the expression of known effectors of centriole synthesis, such as *PLK4*, *STIL*, *CEP152*, *SASS6*, but also of cell cycle regulators, such as *CDK1*, *CCNB1*, *CDC20*, *SGOL2* and *NEK2* (Fig. 1d and Supplementary Fig. 1). We reasoned that uncharacterized cell cycle-related genes that are specific to this subpopulation could encode new components of the deuterosome-dependent centriole amplification pathway. A particularly interesting candidate in this category was *CDC20B* (Fig. 1d), which is related to the cell cycle regulators *CDC20* and *FZR1*[12] (Supplementary Fig. 2a). First, the *CDC20B* gene is present in the vertebrate genomic locus that also contains the key MCC regulators *MCIDAS*[9] and *CCNO*[8]. Co-expression of *CDC20B*, *MCIDAS* and *CCNO*

throughout HAEC differentiation was indeed observed in an independent RNA sequencing study, performed on a bulk population of HAECs (Supplementary Fig. 2c). These results fit well with the observation that the promoter of human *CDC20B* was strongly activated by the MCIDAS partners E2F1 and E2F4 (Supplementary Fig. 2d), as also shown in *Xenopus* by others[13] (Supplementary Fig. 2e). Second, the *CDC20B* gene bears in its second intron the miR-449 microRNAs (Supplementary Fig. 3k), which were shown to contribute to MCC differentiation[10, 14-17]. Finally, in *Xenopus* epidermal MCCs, *cdc20b* transcripts were specifically detected during the phase of centriole amplification (Supplementary Fig. 3a-i). This first set of data pointed out the specific and conserved expression pattern of *CDC20B* in immature MCCs, and prompted us to analyze its putative role in centriole amplification.

We then analyzed the subcellular localization of CDC20B protein in human, mouse and *Xenopus* MCCs. As previously reported, the CDC20B protein was detected near BBs[10], but also in cilia of fully differentiated human airway MCCs (Supplementary Fig. 2f-h). This was confirmed by proximity ligation assays that revealed a tight association of CDC20B with Centrin2 and acetylated α-tubulin, in BBs and cilia, respectively (Supplementary Fig. 2i-k). In immature mouse tracheal MCCs, double immunofluorescence also revealed the association of CDC20B to Deup1-positive deuterosomes (Fig. 2a and Supplementary Fig. 2b). Likewise, CDC20B decorated deuterosomes, which were revealed by the centriole marker FOP in immature mouse ependymal MCCs (Fig. 2b). Finally, we found that RFP-Cdc20b localized around GFP-Deup1 positive structures in immature *Xenopus* epidermal MCCs (Fig. 2c). We conclude that in vertebrate MCCs, CDC20B is associated to deuterosomes during the phase of centriole production.

Next, *Cdc20b* was knocked down in mouse ependymal MCCs, through post-natal brain electroporation of three distinct shRNAs (Supplementary Fig. 3j). One of them, sh274, which targets the junction between exons 3 and 4, and can therefore only interact with mature

mRNA, was useful to rule out possible interference with the production of miR-449 molecules from the *CDC20B* pre-mRNA (Supplementary Fig. 3j). Despite the reduced expression of CDC20B by all three shRNAs (Fig. 3c), MCC identity was not affected as revealed by FOXJ1 expression (Fig. 3a,b,d). In sharp contrast to control shRNA (Fig. 3e), *Cdc20b* shRNAs caused 50% to 70% of abnormal deuterosomal figures in early stage MCCs, including stalled, fused, oversized or minute deuterosomes (Fig. 3f-h). Late stage CDC20B-deficient ependymal MCCs did not undergo proper multiciliogenesis, and often displayed few centrioles and aberrant deuterosomal figures, suggesting a blockage in the centriole biosynthesis pathway (Fig. 3i-k).

Cdc20b was also knocked down in *Xenopus* epidermal MCCs, through injection of two independent morpholino antisense oligonucleotides targeting either the ATG (Mo ATG), or the exon 1/intron 1 junction (Mo Spl) (Supplementary Fig. 3k). The efficiency of Mo ATG was verified through fluorescence extinction of co-injected *cdc20b-GFP* mRNA (Supplementary Fig. 3m). RT-PCR confirmed that Mo Spl caused intron 1 retention (Supplementary Fig. 3l), which is expected to introduce a premature stop codon, and to produce a Cdc20b protein lacking 96% of its amino-acids, likely to undergo unfolded protein response-mediated degradation. Thus, both morpholinos were expected to generate severe loss of Cdc20b function. We verified that neither morpholinos caused *p53* transcript up-regulation (Supplementary Fig. 3n), a non-specific response to morpholinos that is sometimes detected in zebrafish embryos[18]. Importantly, whole-mount *in situ* hybridization indicated that miR-449 expression was not perturbed in the presence of either morpholinos (Supplementary Fig. 3o). We found that *cdc20b* knockdown did not interfere with acquisition of the MCC fate (Supplementary Fig. 4a-e), but severely impaired multiciliogenesis, as revealed by immunofluorescence and electron microscopy (Fig. 4a-i). This defect stemmed from a dramatic reduction in the number of centrioles, and poor docking at the plasma membrane

(Fig. 4g-o and Supplementary Fig. 4f-k). Late-stage morphant MCCs that lacked cilia often displayed stalled deuterosomal figures, again suggesting a blockage in the centriole biosynthesis pathway (Fig. 5l and Supplementary Fig. 4h). Importantly, centrioles and cilia were rescued in Mo Spl MCCs by co-injection of *cdc20b*, *venus-cdc20b* or *cdc20b-venus* mRNAs (Fig. 4j-o and Supplementary Fig. 4f-k). In normal condition, *Xenopus* epidermal MCCs arise in the inner mesenchymal layer and intercalate into the outer epithelial layer, while the process of centriole amplification is underway. To rule out secondary defects due to poor radial intercalation, we assessed the consequences of *cdc20b* knockdown in MCCs induced in the outer layer by Multicilin overexpression[9]. Like in natural MCCs, Cdc20b proved to be essential for the production of centrioles and cilia in response to Multicilin activity (Supplementary Fig. 5a-g). We also noted that the apical actin network that normally surrounds BBs was not maintained in absence of Cdc20b, although this defect could be secondary to the absence of centrioles (Supplementary Fig. 5d-g). Altogether our functional assays indicate that CDC20B is required for the production of multiple centrioles in vertebrate MCCs.

CDC20B encodes a protein of about 519 amino-acids largely distributed across the vertebrate phylum[10]. In its C-terminal half, CDC20B contains seven well conserved WD40 repeats, predicted to form a β-propeller, showing 49% and 37% identity to CDC20 and FZR1 repeats, respectively (Supplementary Fig. 2a). While CDC20 and FZR1 bind and activate the Anaphase Promoting Complex (APC/C), CDC20B lacks canonical APC/C binding domains (Supplementary Fig. 2a), suggesting a distinct molecular function. Insight into this function was suggested by an unbiased interactome study, which reported an association of CDC20B with the mitotic kinase PLK1[19]. Phosphorylation of the pericentriolar material protein Pericentrin (PCNT) by PLK1 induces its cleavage by the protease Separase, thereby allowing centriole disengagement at the end of mitosis[20-22]. Based on our phenotypic observations, we

hypothesized that the PLK1/Separase/PCNT axis could not only control centriole disengagement in mitotic cells, but also centriole release from deuterosomes in MCCs (Fig. 5o). Consistent with this idea, *PLK1*, *Separase* (*ESPL1*), its inhibitor *Securin* (*PTTG1*), and *PCNT* were found to be expressed in human deuterosome-stage MCCs (Supplementary Fig. 1), and/or in *Xenopus* epidermal MCCs[13]. The corresponding proteins were all detected in maturing murine ependymal MCCs (Fig. 5a-f). Of particular relevance, PCNT showed a prominent association to deuterosomes actively engaged in centriole synthesis (Fig. 5f). STED super-resolution fluorescent microscopy further revealed that PCNT was tightly associated to centriolar walls, consistent with a role in the physical maintenance of centrioles around deuterosomes (Fig. 5g). We also note that PLK1 was found enriched around deuterosomes of cultured murine ependymal MCCs prior to centriole disengagement[23]. We functionally tested our hypothesis, by over-expressing human Separase in *Xenopus cdc20b* morphant MCCs to force the release of centrioles from deuterosomes. Over-expression of wild-type, but not protease-dead Separase, efficiently rescued the production of centrioles and cilia in Cdc20b-deficient MCCs (Fig. 5h-n and Supplementary Fig. 5k-p). Separase could also rescue multiciliogenesis in Multicilin-induced MCCs injected with *cdc20b* morpholinos (Supplementary Fig. 5q-w). Interestingly, we noticed that overexpression of Cdc20b or Separase both caused the formation of multipolar spindles in non-MCC dividing cells, consistent with forced centriole disengagement[24] (Supplementary Fig. 5h-j). These results suggest that the function of CDC20B in early-stage MCCs consists of allowing the release by Separase of mature centrioles from deuterosomes.

In this study, we report for the first time the essential and conserved role of CDC20B in vertebrate multiciliogenesis. Our data suggest that the presence of CDC20B around deuterosomes is necessary to allow Separase-dependent proteolysis leading to centriole disengagement. How Separase is activated in maturing MCCs remains to be addressed.

During the cell cycle, Separase is activated through APC/C-mediated degradation of its inhibitor Securin, which involves activation of APC/C by CDC20 or FZR1[12]. We found that *CDC20* and *FZR1* are expressed in human deuterosome-stage MCCs (Fig. 1d and Supplementary Fig. 1). CDC20 protein was detected in cultured murine ependymal MCCs during the phase of centriole disengagement[23], and FZR1 genetic ablation was reported to cause reduced production of centrioles and cilia in mouse ependymal MCCs[25]. Although not formally excluded, direct APC/C activation by CDC20B is unlikely, based on its structure (Supplementary Fig. 2a) and on unbiased interactome studies, which failed to recover interaction with any of the APC/C complex components[19, 26]. APC/C is therefore likely activated in maturing MCCs by its classical partners, CDC20 and/or FZR1, leading to Separase activation through degradation of its inhibitor Securin. Additional factors may contribute to activation of Separase. For instance, we noticed that the APC/C inhibitor FBXO43 (EMI2)[27] is strongly up-regulated in mouse and frog MCCs[13, 28]. As PLK1 is known to induce SCF-mediated degradation of EMI2[29], it could coordinate Separase activation in the cytoplasm and PCNT priming on deuterosomes. Also of interest, SPAG5 (Astrin), a common interactor of DEUP1 and CDC20B[26, 30], was reported to control timely activation of Separase during the cell cycle[24]. It is therefore possible that multiple modes of activation of Separase act in parallel to trigger the release of neo-synthesized centrioles in maturing MCCs. Alternatively, different pathways may be used in distinct species, or in distinct types of MCCs. We found that beyond its association to deuterosomes during the phase of centriole amplification, CDC20B was also associated to basal bodies and cilia in fully differentiated MCCs. This dual localization in mature MCCs is consistent with poor BB apical docking and cilium growth caused by CDC20B knockdown in our models. However, refined temporal and spatial control of CDC20B inhibition will be needed to study its putative role beyond centriole synthesis.

This and previous studies[10, 14-17] establish that the miR-449 cluster and its host gene *CDC20B* are commonly involved in multiciliogenesis. Consistent with its early expression, it was suggested that miR-449 controls cell cycle exit and entry into differentiation of MCCs[10, 15]. This study reveals that CDC20B is involved in the production of centrioles, the first key step of the multiciliogenesis process. From that perspective, the nested organization of miR-449 and *CDC20B* in vertebrate genomes, which allows their coordinated expression, appears crucial for successful multiciliogenesis.

Recently, congenital mutations in MCIDAS and CCNO were shown to cause a newly-recognized MCC-specific disease, called Reduced Generation of Multiple motile Cilia (RGMC), characterized by severe chronic lung infections and increased risk of infertility[7, 8]. Its location in the same genetic locus as MCIDAS and CCNO makes CDC20B a good candidate for RGMC. By extension, new deuterosome-stage specific genes uncovered by scRNA-seq in this study also represent potential candidates for additional RGMC mutations.

Previous works have established the involvement of the centriole duplication machinery active in S-phase of the cell cycle, during centriole multiplication of vertebrate post-mitotic MCCs[3-5]. Our study further reveals a striking analogy between centriole disengagement from deuterosomes in MCCs, and centriole disengagement that occurs during the M/G1 transition of the cell cycle (Fig. 5o). Thus, it appears that centriole production in MCCs recapitulates the key steps of the centriole duplication cycle[31]. However, the cell cycle machinery must adapt to the acentriolar deuterosome to massively produce centrioles. Such adaptation appears to involve physical and functional interactions between canonical cell cycle molecules, such as CEP152 and PLK1, and recently evolved cell cycle-related deuterosomal molecules, such as DEUP1[5] and CDC20B. It remains to examine whether additional deuterosomal molecules have emerged in the vertebrate phylum to sustain massive centriole production in MCCs.

In conclusion, this work illustrates how coordination between ancestral and recently evolved cell cycle-related molecules can give rise to a new differentiation mechanism in vertebrates.

References

1. Spassky, N. & Meunier, A. The development and functions of multiciliated epithelia. *Nature reviews* **18**, 423-436 (2017).
2. Brooks, E.R. & Wallingford, J.B. Multiciliated cells. *Curr Biol* **24**, R973-982 (2014).
3. Al Jord, A. *et al.* Centriole amplification by mother and daughter centrioles differs in multiciliated cells. *Nature* **516**, 104-107 (2014).
4. Klos Dehring, D.A. *et al.* Deuterosome-mediated centriole biogenesis. *Developmental cell* **27**, 103-112 (2013).
5. Zhao, H. *et al.* The Cep63 paralogue Deup1 enables massive de novo centriole biogenesis for vertebrate multiciliogenesis. *Nature cell biology* **15**, 1434-1444 (2013).
6. Meunier, A. & Azimzadeh, J. Multiciliated Cells in Animals. *Cold Spring Harbor perspectives in biology* **8** (2016).
7. Boon, M. *et al.* MCIDAS mutations result in a mucociliary clearance disorder with reduced generation of multiple motile cilia. *Nature communications* **5**, 4418 (2014).
8. Wallmeier, J. *et al.* Mutations in CCNO result in congenital mucociliary clearance disorder with reduced generation of multiple motile cilia. *Nature genetics* **46**, 646-651 (2014).
9. Stubbs, J.L., Vladar, E.K., Axelrod, J.D. & Kintner, C. Multicilin promotes centriole assembly and ciliogenesis during multiciliate cell differentiation. *Nature cell biology* **14**, 140-147 (2012).
10. Marcet, B. *et al.* Control of vertebrate multiciliogenesis by miR-449 through direct repression of the Delta/Notch pathway. *Nature cell biology* **13**, 693-699 (2011).
11. Tan, F.E. *et al.* Myb promotes centriole amplification and later steps of the multiciliogenesis program. *Development (Cambridge, England)* **140**, 4277-4286 (2013).
12. Yu, H. Cdc20: a WD40 activator for a cell cycle degradation machine. *Molecular cell* **27**, 3-16 (2007).
13. Ma, L., Quigley, I., Omran, H. & Kintner, C. Multicilin drives centriole biogenesis via E2f proteins. *Genes & development* **28**, 1461-1471 (2014).
14. Song, R. *et al.* miR-34/449 miRNAs are required for motile ciliogenesis by repressing cp110. *Nature* **510**, 115-120 (2014).
15. Otto, T. *et al.* Cell cycle-targeting microRNAs promote differentiation by enforcing cell-cycle exit. *Proceedings of the National Academy of Sciences of the United States of America* (2017).
16. Wu, J. *et al.* Two miRNA clusters, miR-34b/c and miR-449, are essential for normal brain development, motile ciliogenesis, and spermatogenesis. *Proceedings of the National Academy of Sciences of the United States of America* **111**, E2851-2857 (2014).
17. Chevalier, B. *et al.* miR-34/449 control apical actin network formation during multiciliogenesis through small GTPase pathways. *Nature communications* **6**, 8386 (2015).

18. Robu, M.E. *et al.* p53 activation by knockdown technologies. *PLoS genetics* **3**, e78 (2007).
19. Huttlin, E.L. *et al.* The BioPlex Network: A Systematic Exploration of the Human Interactome. *Cell* **162**, 425-440 (2015).
20. Kim, J., Lee, K. & Rhee, K. PLK1 regulation of PCNT cleavage ensures fidelity of centriole separation during mitotic exit. *Nature communications* **6**, 10076 (2015).
21. Matsuo, K. *et al.* Kendrin is a novel substrate for separase involved in the licensing of centriole duplication. *Curr Biol* **22**, 915-921 (2012).
22. Tsou, M.F. *et al.* Polo kinase and separase regulate the mitotic licensing of centriole duplication in human cells. *Developmental cell* **17**, 344-354 (2009).
23. Al Jord, A. *et al.* Calibrated mitotic oscillator drives motile ciliogenesis. *Science* (2017).
24. Thein, K.H., Kleylein-Sohn, J., Nigg, E.A. & Gruneberg, U. Astrin is required for the maintenance of sister chromatid cohesion and centrosome integrity. *The Journal of cell biology* **178**, 345-354 (2007).
25. Eguren, M. *et al.* The APC/C cofactor Cdh1 prevents replicative stress and p53-dependent cell death in neural progenitors. *Nature communications* **4**, 2880 (2013).
26. Rual, J.F. *et al.* Towards a proteome-scale map of the human protein-protein interaction network. *Nature* **437**, 1173-1178 (2005).
27. Tischer, T., Hormanseder, E. & Mayer, T.U. The APC/C inhibitor XErp1/Emi2 is essential for Xenopus early embryonic divisions. *Science* **338**, 520-524 (2012).
28. Hoh, R.A., Stowe, T.R., Turk, E. & Stearns, T. Transcriptional program of ciliated epithelial cells reveals new cilium and centrosome components and links to human disease. *PLoS ONE* **7**, e52166 (2012).
29. Hansen, D.V., Tung, J.J. & Jackson, P.K. CaMKII and polo-like kinase 1 sequentially phosphorylate the cytostatic factor Emi2/XErp1 to trigger its destruction and meiotic exit. *Proceedings of the National Academy of Sciences of the United States of America* **103**, 608-613 (2006).
30. Firat-Karalar, E.N., Rauniyar, N., Yates, J.R., 3rd & Stearns, T. Proximity interactions among centrosome components identify regulators of centriole duplication. *Curr Biol* **24**, 664-670 (2014).
31. Firat-Karalar, E.N. & Stearns, T. The centriole duplication cycle. *Philosophical transactions of the Royal Society of London* **369** (2014).
32. Qiu, X. *et al.* Reversed graph embedding resolves complex single-cell trajectories. *Nature methods* (2017).
33. Macosko, E.Z. *et al.* Highly Parallel Genome-wide Expression Profiling of Individual Cells Using Nanoliter Droplets. *Cell* **161**, 1202-1214 (2015).
34. Kim, D. *et al.* TopHat2: accurate alignment of transcriptomes in the presence of insertions, deletions and gene fusions. *Genome biology* **14**, R36 (2013).
35. Anders, S., Pyl, P.T. & Huber, W. HTSeq--a Python framework to work with high-throughput sequencing data. *Bioinformatics (Oxford, England)* **31**, 166-169 (2015).
36. Love, M.I., Huber, W. & Anders, S. Moderated estimation of fold change and dispersion for RNA-seq data with DESeq2. *Genome biology* **15**, 550 (2014).
37. Langmead, B. & Salzberg, S.L. Fast gapped-read alignment with Bowtie 2. *Nature methods* **9**, 357-359 (2012).

38. Heinz, S. *et al.* Simple combinations of lineage-determining transcription factors prime cis-regulatory elements required for macrophage and B cell identities. *Molecular cell* **38**, 576-589 (2010).
39. Boutin, C. *et al.* A dual role for planar cell polarity genes in ciliated cells. *Proceedings of the National Academy of Sciences of the United States of America* **111**, E3129-3138 (2014).
40. Boutin, C. *et al.* NeuroD1 induces terminal neuronal differentiation in olfactory neurogenesis. *Proceedings of the National Academy of Sciences of the United States of America* **107**, 1201-1206 (2010).
41. Boutin, C., Diestel, S., Desoeuvre, A., Tiveron, M.C. & Cremer, H. Efficient in vivo electroporation of the postnatal rodent forebrain. *PLoS ONE* **3**, e1883 (2008).
42. You, Y. & Brody, S.L. Culture and Differentiation of Mouse Tracheal Epithelial Cells, in *Epithelial Cell Culture Protocols* 123-143 (Springer, 2012).
43. Marchal, L., Luxardi, G., Thome, V. & Kodjabachian, L. BMP inhibition initiates neural induction via FGF signaling and Zic genes. *Proceedings of the National Academy of Sciences of the United States of America* **106**, 17437-17442 (2009).
44. Castillo-Briceno, P. & Kodjabachian, L. Xenopus embryonic epidermis as a mucociliary cellular ecosystem to assess the effect of sex hormones in a non-reproductive context. *Frontiers in zoology* **11**, 9 (2014).
45. Deblandre, G.A., Wettstein, D.A., Koyano-Nakagawa, N. & Kintner, C. A two-step mechanism generates the spacing pattern of the ciliated cells in the skin of Xenopus embryos. *Development (Cambridge, England)* **126**, 4715-4728 (1999).

Acknowledgements

We are grateful to Chris Kintner, Marc Kirschner, Olaf Stemmann, Reinhard Köster, Xavier Morin and Xueliang Zhu for reagents. Imaging in IBDM was performed on PiCSL-FBI core facility, supported by the French National Research Agency through the program "Investments for the Future" (France-BioImaging, ANR-10-INBS-04). Sequencing at UCAGenomiX (IPMC), a partner of the National Infrastructure France Génomique, was supported by Commissariat aux Grands Investissements (ANR-10-INBS-09-03, ANR-10-INBS-09-02) and Cancerop̂le PACA. The authors thank Florian Roguet for *Xenopus* care, and Nathalie Garin from Leica Microsystems GmbH for technical advice on STED microscopy. We are grateful to Rainer Waldmann, Kévin Lebrigand and Nicolas Nottet for fruitful discussions on single cell RNA sequencing. We thank Julien Royet and Harold Cremer for insightful comments on the manuscript. This project was funded by grants from

ANR (ANR-11-BSV2-021-02, ANR-13-BSV4-0013, ANR-15-CE13-0003), FRM (DEQ20141231765, DEQ20130326464), Fondation ARC (PJA 20161204865, PJA 20161204542), the labex Signalife (ANR-11-LABX-0028-01), and the association Vaincre la Mucoviscidose (RF20140501158, RF20120600738, RF20150501288). OM, CB and DRR were supported by fellowships from Ligue Nationale contre le Cancer (OM and CB), and Fondation ARC (DRR).

Author contributions

PB, BM and LK designed and supervised the study, and obtained funding. LEZ, SRG, OM performed and analyzed human and mouse airway cells experiments. DRR and VT performed and analyzed *Xenopus* experiments. CB performed and analyzed experiments on mouse ependymal MCCs. OR performed WB analysis. MD and AP performed the bioinformatic analysis. All authors were involved in data interpretation. DRR, LEZ and CB designed the figures. LK, PB, DRR, LEZ, CB, and BM wrote the manuscript.

Competing financial interests

The authors declare no competing financial interests.

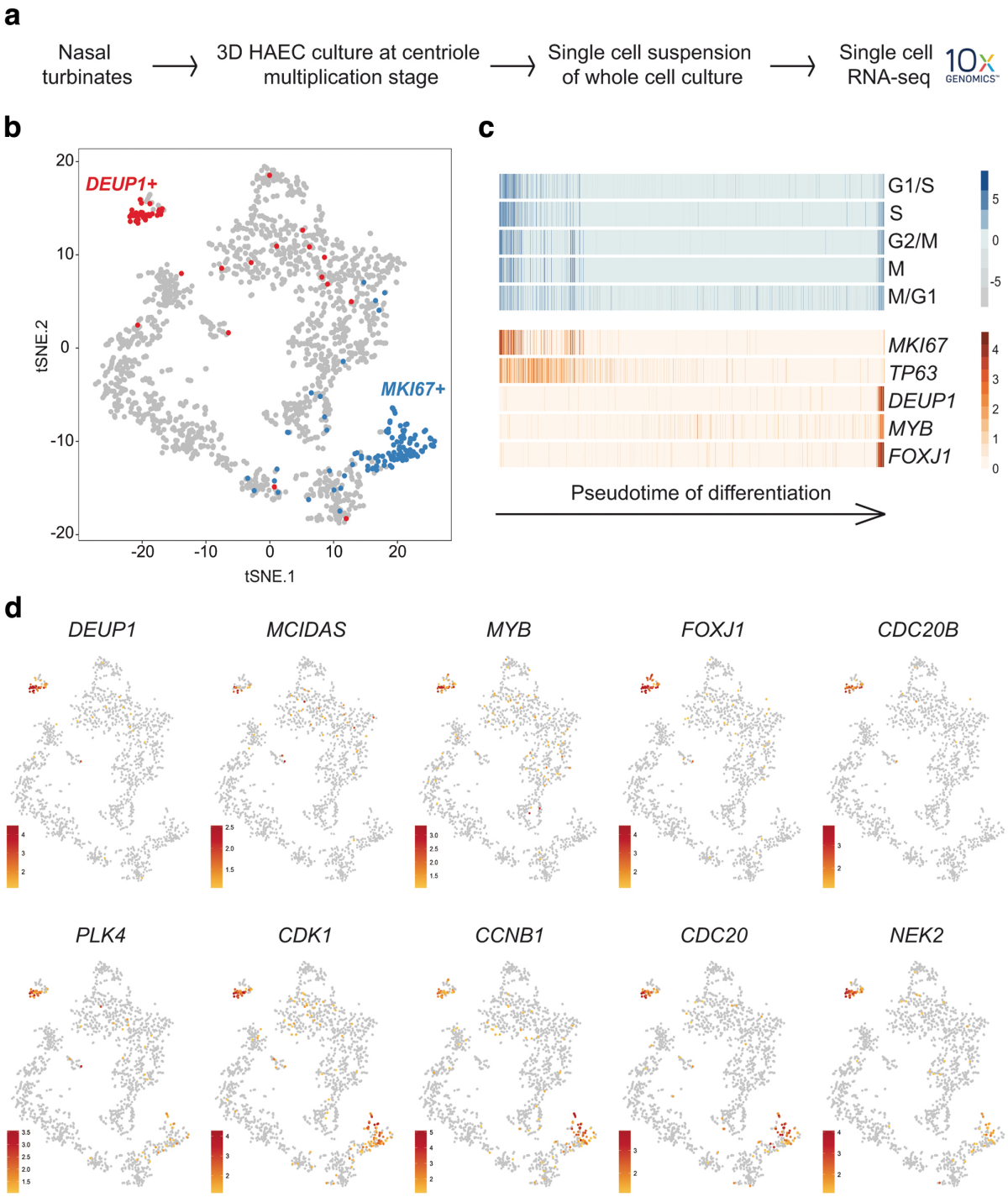

Figure 1: Single-cell RNA-seq analysis reveals *CDC20B* as a novel specific marker of deuterosomal stage MCCs, and enrichment of cell cycle-related genes in this cell population.

(**a**) Experimental design of the scRNA-seq experiment. (**b**) tSNE plot. Each point is a projection of a unique cell on a 2D space generated by the tSNE algorithm. Blue dots represent *MKI67*-positive proliferating cells, and red dots represent *DEUP1*-positive cells

corresponding to maturing MCCs at deuterosome stage. (**c**) Cell cycle-related gene set expression in HAECs measured by scRNA-seq. Cells were ordered along a pseudotime axis, defined with the Monocle2 package. Phase specific scores are displayed in the top heatmap. Expression of selected genes is displayed in the bottom heatmap. (**d**) tSNEs plots for a selection of genes specifically enriched in deuterosome-stage cells. Note that *CDC20B* exhibits the most specific expression among deuterosome marker genes.

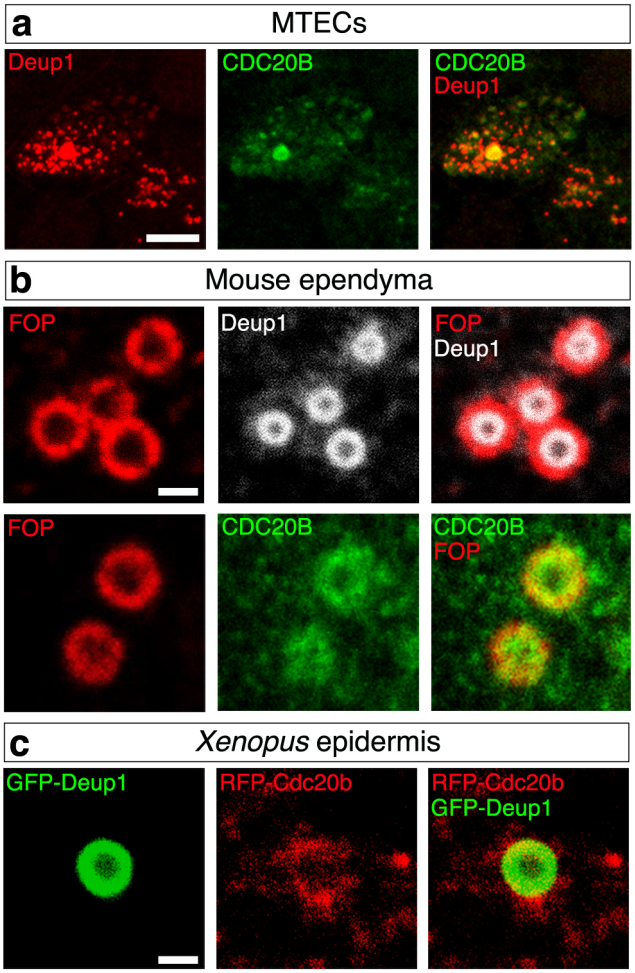

Figure 2: CDC20B is a component of the vertebrate deuterosome

(**a**) Double immunofluorescence was performed on mouse tracheal epithelial cells (MTECs) after 3 days of culture in air-liquid interface. High magnification confocal pictures of maturing MCCs revealed the association of CDC20B protein to deuterosomes marked by Deup1. (**b**) Maturing mouse ependymal MCCs were immunostained as indicated, and high magnification confocal pictures were taken. In these cells, centrioles revealed by FOP form a ring around deuterosomes marked by Deup1. CDC20B staining forms a ring inside the ring of FOP-positive centrioles, indicating that CDC20B is tightly associated to deuterosomes. (**c**) *Xenopus* embryos were injected with *MCI-hGR, GFP-Deup1* and *RFP-cdc20b* mRNAs, treated with dexamethasone at gastrula st11 to induce Multicilin activity, and immunostained at neurula st18 as indicated. Scale bars: 5µm (**a**), 1µm (**b**,**c**).

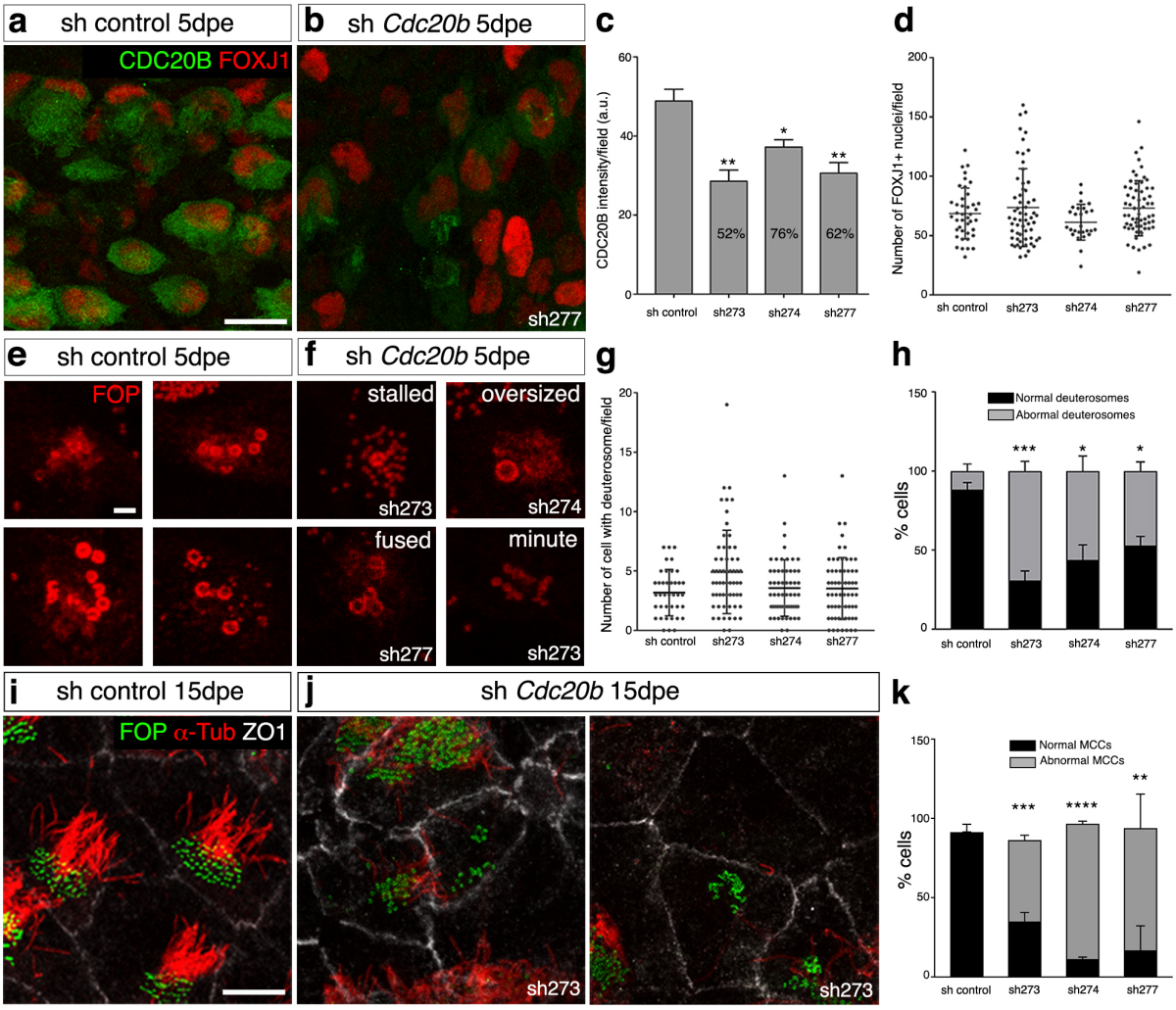

Figure 3: CDC20B knockdown affects the production of centrioles and cilia in mouse ependymal MCCs.

(**a**,**b**) Ependyma were stained for CDC20B (green) and FOXJ1 (nuclear MCC fate marker, red) 5 days post electroporation (5dpe) of control shRNA (**a**) or *Cdc20b* shRNA (**b**). sh277 is exemplified here, but all three *Cdc20b* shRNAs produced similar effects. (**c**) Bar graph showing the quantification of CDC20B protein levels after *in vivo* electroporation of anti-*Cdc20b* shRNAs. Percentage of expression relative to sh control is indicated on anti-*Cdc20b* sh bars. (**d**) Histogram showing the number of FOXJ1-positive nuclei observed for each field (dot), with mean values (horizontal lines) and standard deviations (vertical lines). No significant variations were observed between conditions, indicating that MCC fate acquisition was not affected by *Cdc20b* knockdown. (**e**-**h**) FOP immunostaining was used to analyse

deuterosomal figures in 5dpe ependymal MCCs electroporated with control shRNA (**e**) or *Cdc20b* shRNAs (**f**). Various examples of normal deuterosomal figures are shown in (**e**) and examples of abnormal deuterosomal figures caused by *Cdc20b* knockdown are shown in (**f**). Stalled, oversized, fused and minute deuterosomes were typical defects commonly caused by all three *Cdc20b* shRNAs. (**g**) Histogram showing the number of cells with deuterosomal figures observed for each field (dots), with mean values (horizontal bars) and standard deviations (vertical lines). (**h**) Bar graph showing the percentage of cells, which displayed normal and abnormal deuterosomal figures in each condition. *Cdc20b* knockdown by all three shRNAs caused significant increase in the number of abnormal deuterosomal figures. (i-j) Confocal pictures of 15dpe ependyma stained for FOP (centrioles, green), α-tubulin (cilia, red) and ZO1 (cell junction, white) showing the morphology of normal MCCs in sh control condition (**i**), and examples of abnormal MCCs observed in sh *Cdc20b* conditions (**j**). (**k**) Bar graph showing the percentage of normal and abnormal MCCs, as revealed by staining of centrioles and cilia. Scale bars: 1μm (**a**), 5μm (**e**,**i**).

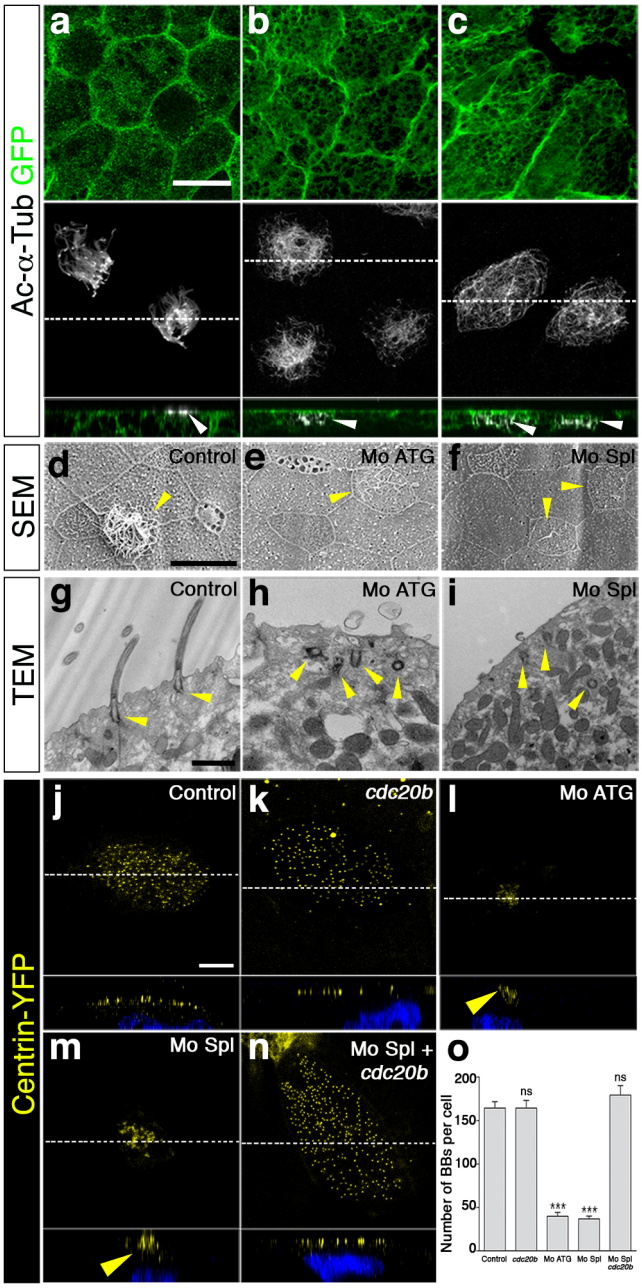

Figure 4: *cdc20b* knockdown impairs centriole multiplication, docking and ciliogenesis in *Xenopus* epidermal MCCs.

(**a-c**) 8-cell embryos were injected in presumptive epidermis with *GFP-CAAX* mRNA and *cdc20b* morpholinos, as indicated. Embryos at tailbud st25 were processed for fluorescent staining against GFP (injection tracer, green) and Acetylated α-Tubulin (cilia, white). White dotted lines indicate the position of orthogonal projections shown in bottom panels. Note that

cdc20b morphant MCCs display cytoplasmic filaments but do not grow cilia (white arrowheads). (**d-f**) Scanning Electron Microscopy (SEM) of control (**d**) and *cdc20b* morphant (**e**,**f**) embryos at tadpole st31. Yellow arrowheads point at normal (**d**) and defective MCCs (**e**,**f**). (**g-i**) Transmission Electron Microscopy (TEM) of control (**g**) and *cdc20b* morphant (**h**,**i**) embryos at tailbud st25. Yellow arrowheads point at normally docked basal bodies supporting cilia (**g**) and undocked centrioles unable to support cilia (**h**,**i**). (**j-n**) 8-cell embryos were injected in presumptive epidermis with *centrin-YFP* mRNA, *cdc20b* morpholinos, and *cdc20b* mRNA, as indicated. Centrin-YFP fluorescence was observed directly to reveal centrioles (yellow). Nuclei were revealed by DAPI staining in blue. White dotted lines indicate the position of orthogonal projections shown in bottom panels. Yellow arrowheads point at undocked centrioles. (**o**) Bar graph showing the number of BBs per MCC, as counted by Centrin-YFP dots. *cdc20b* knockdown significantly reduced the number of BBs per cell, and this defect could be corrected by *cdc20b* co-injection with Mo Spl. Scale bars: 20µm (**a**,**d**); 1µm (**g**); 5µm (**j**).

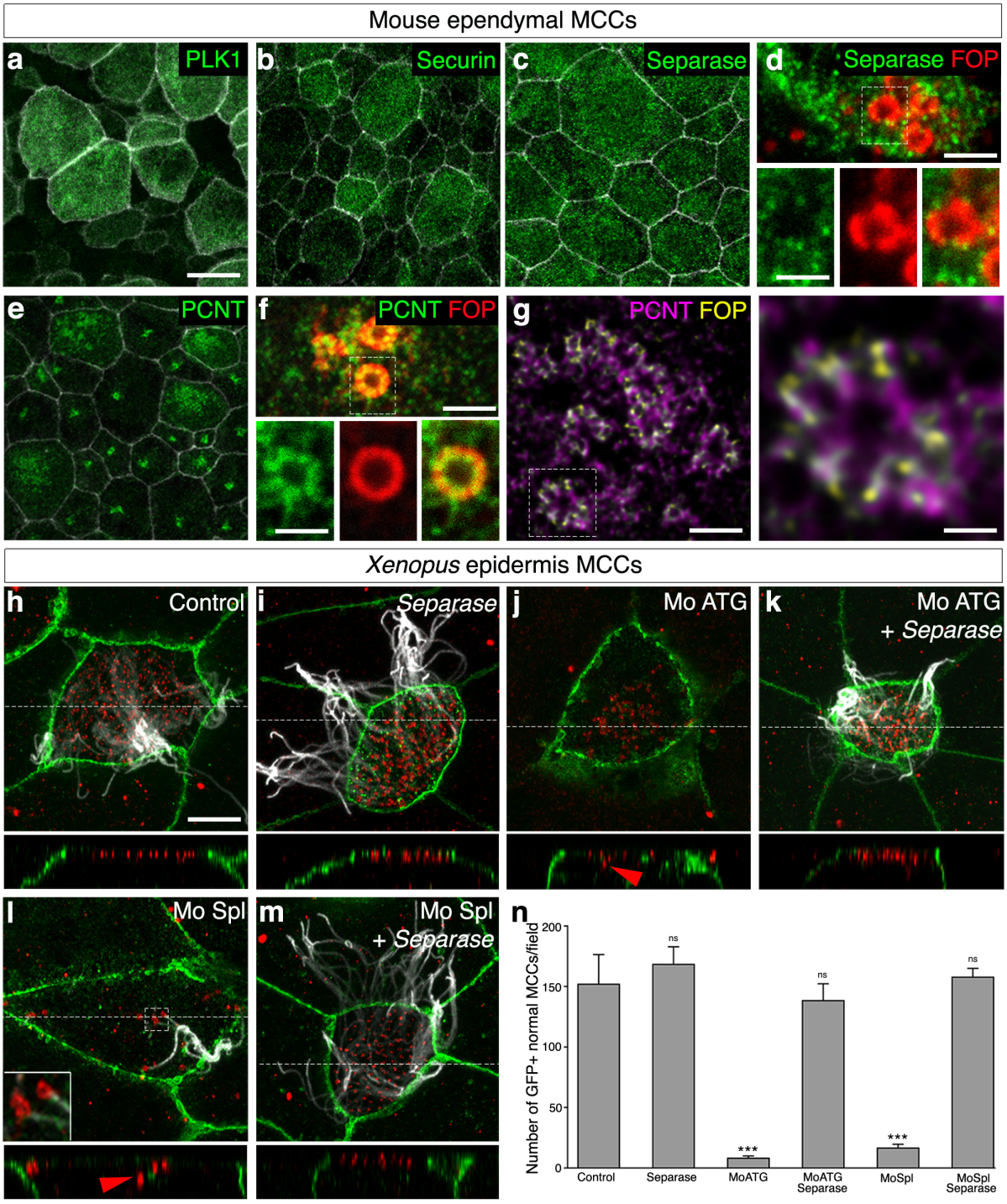

Figure 5: Separase overexpression rescues multiciliogenesis in absence of CDC20B.

(**a**-**f**) Maturing mouse ependyma were immunostained for ZO1 (white) and indicated proteins, and photographed with a confocal microscope. PLK1, Separase, Securin and PCNT were all expressed in maturing MCCs, which can be identified due to their large apical area. High magnifications show that Separase (**d**) and PCNT (**f**) localize in the vicinity of deuterosomes marked by FOP. (**g**) STED picture showing the organization of PCNT (magenta) and FOP (yellow) around deuterosomes. (**h**-**m**) 8-cell *Xenopus* embryos were injected in the presumptive epidermis with *GFP-CAAX* mRNA, *cdc20b* morpholinos, and human *Separase* mRNA, as indicated. Embryos were fixed at tailbud st25 and immunostained against GFP (injection tracer, green), Acetylated α-Tubulin (cilia, white) and ɣ-tubulin (BBs, red). White dotted lines indicate the position of orthogonal projections shown in bottom panels. Red arrowheads point undocked BBs. Left inset in (**l**) shows zoom on stalled deuterosomal figures. (**n**) Bar graph showing the number of properly ciliated MCCs among injected cells, per field of observation. Separase overexpression fully rescued multiciliogenesis in *cdc20b* morphant MCCs. Scale bars: 10µm (**a**); 5µm (**c**,**f**, top), 1µm (**c**,**f**, bottom), 2µm (**g**, left), 500nm (**g**, right), 5µm (**h**-**m**). (**o**) Model illustrating the analogy between centriole disengagement in mitotic cells and centriole release from deuterosomes in post-mitotic MCCs.

Materials and Methods

Subjects/human samples

Inferior turbinates were from patients who underwent surgical intervention for nasal obstruction or septoplasty (provided by L. Castillo, Nice University Hospital, France). The use of human tissues was authorized by the bioethical law 94-654 of the French Public Health Code and written consent from the patients.

Single-cell RNA sequencing of HAECs

HAECs were cultured as previously described [10]. They were induced to differentiate at the air-liquid interface for 14 days, which corresponds to the maximum centriole multiplication stage. Cells were incubated on Transwell® (Corning®, NY 14831 USA) with 0.1% protease type XIV from *Streptomyces griseus* (Sigma-Aldrich) in HBSS (Hanks' balanced salts) for 4 hours at 4°C degrees. Cells were gently detached from the Transwells by pipetting and then transferred to a microtube. 50 units of DNase I (EN0523 Thermo Fisher Scientific) per 250µl, were directly added and cells were further incubated at room temperature for 10 min. Cells were centrifuged (150g for 5 min) and resuspended in 500 µL HBSS 10% Fetal Bovine Serum (Gibco), centrifuged again (150g for 5 min) and resuspended in 500 µL HBSS before being mechanically dissociated through a 26G syringe (4 times). Finally, cell suspensions were filtered through a Scienceware® Flowmi™ Cell Strainer (40µm porosity), centrifuged (150g for 5 min) and resuspended in 500 µL of cold HBSS. Cell concentration measurements were performed with Scepter™ 2.0 Cell Counter (millipore) and Countess™ automated cell counter (ThermoFisher Scientific). Cell viability was checked with Countess™ automated cell counter (ThermoFisher Scientific). All steps except the DNAse I incubation were performed on ice. For the cell capture by the 10X genomics device, the cell concentration was adjusted to 300 cells/µl in HBSS aiming to capture 1500 cells. We then followed the

manufacturer's protocol (Chromium™ Single Cell 3' Reagent Kit, v2 Chemistry) to obtain single cell 3' libraries for Illumina sequencing. Libraries were sequenced with a NextSeq 500/550 High Output v2 kit (75 cycles) that allows up to *91* cycles of paired-end sequencing: the forward read had a length of 26 basse that included the cell barcode and the UMI; the reverse read had a length of 57 bases that contained the cDNA insert. CellRanger Single-Cell Software Suite v1.3 was used to perform sample demultiplexing, barcode processing and single-cell 3′ gene counting using standards default parameters and human build hg19. Additional analyses were performed using R. Pseudotemporal ordering of single cells was performed with the last release of the Monocle package [32]. Cell cycle scores were calculated by summing the normalized intensities of genes belonging to phase-specific gene sets then centered and scaled by phase. Gene sets for each phase were curated from previously described sets of genes [33](Table S1). Data was submitted to the GEO portal under series reference GSE103518. Data shown in Figure 1 is representative of 4 independent experiments performed on distinct primary cultures.

RNA sequencing of HAECs

For Figure S3A, three independent HAEC cultures (HAEC1, HAEC2, HAEC3) were triggered to differentiate in air-liquid interface (ALI) cultures for 2 days (ALI day 2, undifferentiated), ALI day 14 (first cilia) or ALI day 28 (well ciliated). RNA was extracted with the miRNeasy mini kit (Qiagen) following manufacturer's instructions. mRNA-seq was performed from 2 µg of RNA that was first subjected to mRNA selection with Dynabeads® mRNA Purification Kit (Invitrogen). mRNA was fragmented 10 min at 95°C in RNAseIII buffer (Invitrogen) then adapter-ligated, reverse transcribed and amplified (6 cycles) with the reagents from the NEBNext Small RNA Library Prep Set for SOLiD. Small RNA-seq was performed from 500 ng RNA with the NEBNext Small RNA Library Prep Set for SOLiD (12

PCR cycles) according to manufacturer's instructions. Both types of amplified libraries were purified on Purelink PCR micro kit (Invitrogen), then subjected to additional PCR rounds (8 cycles for RNA-seq and 4 cycles for small RNA-seq) with primers from the 5500 W Conversion Primers Kit (Life Technologies). After Agencourt® AMPure® XP beads purification (Beckman Coulter), libraries were size-selected from 150 nt to 250 nt (for RNA-seq) and 105 nt to 130 nt (for small RNA-seq) with the LabChip XT DNA 300 Assay Kit (Caliper Lifesciences), and finally quantified with the Bioanalyzer High Sensitivity DNA Kit (Agilent). Libraries were sequenced on SOLiD 5500XL (Life Technologies) with single-end 50b reads. SOLiD data were analyzed with lifescope v2.5.1, using the small RNA pipeline for miRNA libraries and whole transcriptome pipeline for RNA-seq libraries with default parameters. Annotation files used for production of raw count tables correspond to Refseq Gene model v20130707 for mRNAs and miRBase v18 for small RNAs. Data generated from RNA sequencing were then analyzed with Bioconductor (http://www.bioconductor.org) package DESeq and size-factor normalization was applied to the count tables. Heatmaps were generated with GenePattern using the "Hierarchical Clustering" Module, applying median row centering and Euclidian distance.

Re-analysis of *Xenopus* E2F4 Chip-seq and RNA-seq

RNA-seq (samples GSM1434783 to GSM1434788) and ChIP-seq (samples GSM1434789 to GSM1434792) data were downloaded from GSE59309. Reads from RNA-seq were aligned to the *Xenopus laevis* genome release 7.1 using TopHat2 [34] with default parameters. Quantification of genes was then performed using HTSeq-count [35] release 0.6.1 with "-m intersection-nonempty" option. Normalization and statistical analysis were performed using Bioconductor package DESeq2 [36]. Differential expression analysis was done between Multicilin-hGR alone versus Multicilin-hGR in the presence of E2f4ΔCT. Reads from ChIP-

seq were mapped to the *Xenopus laevis* genome release 7.1 using Bowtie2 [37]. Peaks were called and annotated according to their positions on known exons with HOMER [38]. Peak enrichments of E2F4 binding site in the promoters of centriole genes and cell cycle genes [13] were estimated in presence or absence of Multicilin and a ratio of E2F4 binding (Multicilin vs no Multicilin) was calculated.

Promoter reporter studies

The human *CDC20B* promoter was cloned into the pGL3 Firefly Luciferase reporter vector (Promega) with SacI and NheI cloning sites. The promoter sequenced ranged from -1073 to +104 relative to the transcription start site. 37.5 ng of pGL3 plasmid were applied per well. pCMV6-Neg, pCMV6-E2F1 (NM_005225) and pCMV6-E2F4 (NM_001950) constructs were from Origene. 37.5 ng of each plasmid was applied per well. 25 ng per well of pRL-CMV (Promega) was applied in the transfection mix for transfection normalization (Renilla luciferase). HEK 293T cells were seeded at 20 000 cells per well on 96-well plates. The following day, cells were transfected with the indicated plasmids (100 ng of total DNA) with lipofectamine 3000 (Invitrogen). After 24 hours, cells were processed with the DualGlo kit (Promega) and luciferase activity was recorded on a plate reader.

Proximity ligation Assays

Fully differentiated HAECs were dissociated by incubation with 0.1% protease type XIV from *Streptomyces griseus* (Sigma-Aldrich) in HBSS (Hanks' balanced salts) for 4 hours at 4°C. Cells were gently detached from the Transwells by pipetting and then transferred to a microtube. Cells were then cytocentrifuged at 300 rpm for 8 min onto SuperFrostPlus slides using a Shandon Cytospin 3 cytocentrifuge. Slides were fixed for 10 min in methanol at -20°C for Centrin2 and ZO1 assays, and for 10 min in 4% paraformaldehyde at room

temperature and then permeabilized with 0.5% Triton X-100 in PBS for 10 min for Acetylated-α-tubulin assays. Cells were blocked with 3% BSA in PBS for 30 min. The incubation with primary antibodies was carried out at room temperature for 2 h. Then, mouse and rabbit secondary antibodies from the Duolink® Red kit (Sigma-Aldrich) were applied and slides were processed according to manufacturer's instructions. Images were acquired using the Olympus Fv10i confocal imaging systems with 60X oil immersion objective and Alexa 647 detection parameters.

Mice

Timed pregnant CD1 mice were used (Charles Rivers, Lyon, France). Animal experiments were carried out in accordance to European Community Council Directive and approved by French ethical committees (comité d'éthique pour l'expérimentation animale n°14; permission number: 62-12112012).

Immunostaining on mouse ependyma

Immunostaining on ependyma preparations were performed as previously described [39]. Briefly, dissected brains were subjected to 12 min fixation in 4% paraformaldehyde, 0.1% Triton X-100, blocked 1 hour in PBS, 3% BSA, incubated overnight with primary antibodies diluted in PBS, 3% BSA, and incubated 1 h with secondary antibodies at room temperature. Ependyma were dissected further and mounted with Mowiol before imaging using an SP8 confocal microscope (Leica microsystems) equipped with a 63x oil objective. The same protocol was used to prepare samples for super-resolution acquisition. Pictures were acquired with a TCS SP8 STED 3X microscope equipped with an HC PL APO 93X/1.30 GLYC motCORR^{TM} objective (Leica microsystems). Pericentrin was revealed using Alexa 514 (detection 535-564nm, depletion 660nm) and FOP was revealed using Alexa 488 (detection

498-531nm, depletion 592nm). Pictures were deconvoluted using Huygens software. Maximum intensity projection of 3 deconvoluted pictures is presented in Figure 4G. Primary antibodies: rabbit anti-CDC20B (1:500; Proteintech), mouse IgG anti-PLK1 (1:500; Thermo Fisher), rabbit anti-Pericentrin (1:500, Abcam), mouse IgG2a anti-Securin (1:100; Abcam), rabbit anti-Separase (1:200; Abcam), mouse IgG1 anti-FoxJ1 (1:1000; eBioscience), rabbit anti-Deup1 (1:1000; kindly provided by Dr Xueliang Zhu), rabbit anti-ZO1 (1:600; Thermo Fisher Scientific), mouse IgG1 anti-ZO1 (1:600; Invitrogen), mouse IgG2b anti-FGFR1OP (FOP) (1:2000; Abnova), mouse IgG1 anti-α-tubulin (1:500; Sigma-Aldrich). Secondary antibodies: Alexa Fluor 488 goat anti-rabbit (1:800; Thermo Fisher Scientific), Alexa Fluor 647 goat anti-rabbit (1:800; Thermo Fisher Scientific), Alexa Fluor 514 goat anti-rabbit (1:800; Thermo Fisher Scientific), Alexa Fluor 488 goat anti-mouse IgG2b (1:800; Thermo Fisher Scientific), Alexa Fluor 568 goat anti-mouse IgG2b (1:800; Thermo Fisher Scientific), Alexa Fluor 488 goat anti-mouse IgG2a (1:800; Thermo Fisher Scientific), Alexa Fluor 568 goat anti-mouse IgG1 (1:800; Thermo Fisher Scientific), Alexa Fluor 647 goat anti-mouse IgG1 (1:800; Thermo Fisher Scientific).

Mouse constructs

Expression constructs containing shRNA targeting specific sequences in the CDC20B coding sequence under the control of the U6 promoter were obtained from Sigma-Aldrich (ref. TRCN0000088273 (sh273), TRCN0000088274 (sh274), TRCN0000088277 (sh277)). PCX-mcs2-GFP vector (Control GFP) kindly provided by Xavier Morin (ENS, Paris, France), and U6 vector containing a validated shRNA targeting a specific sequence in the NeuroD1 coding sequence [40](Control sh, ref. TRCN0000081777, Sigma-Aldrich) were used as controls for electroporation experiments.

Postnatal mouse brain electroporation

Postnatal mouse brain electroporation was performed as described previously [41]. Briefly, P1 pups were anesthetized by hypothermia. A glass micropipette was inserted into the lateral ventricle, and 2 µl of plasmid solution (concentration 3µg/µl) was injected by expiratory pressure using an aspirator tube assembly (Drummond). Successfully injected animals were subjected to five 95V electrical pulses (50 ms, separated by 950 ms intervals) using the CUY21 edit device (Nepagene, Chiba, Japan), and 10 mm tweezer electrodes (CUY650P10, Nepagene) coated with conductive gel (Signagel, Parker laboratories). Electroporated animals were reanimated in a 37°C incubator before returning to the mother.

Statistical analyses of mouse experiments

Analysis of *Cdc20b* shRNAs efficiency (Fig. 3c): For each field, the intensity of CDC20B fluorescent immunostaining was recorded using ImageJ software and expressed as arbitrary units. Data are mean ± sem. Two independent experiments were analyzed. A minimum of 39 fields per condition was analyzed. n= 3, 4, 5 and 5 animals for sh control, sh273, sh274 and sh277, respectively. Unpaired t test vs sh control: p=0.0036 (sh273, **), 0.0135 (sh274, *), 0.0035 (sh277, **).

Analysis of the number of FOXJ1 positive cells at 5dpe (Fig. 3d): Unpaired t test vs sh control: 0.3961 (sh273, ns), 0.1265 (sh274, ns), 0.3250 (sh277, ns).

Analysis of the number of deuterosomal figures at 5dpe (Fig. 3g): 50-100 cells with deuterosomal figures were analyzed per condition. n= 3 4, 2, and 3 animals for sh control, sh273, sh274 and sh277, respectively. Unpaired t test vs sh control: p=0.0059 (sh273, **), 0.4091 (sh274, ns), 0.4805 (sh277, ns). sh273 caused significant increase in the number of deuterosomal figures.

Analysis of deuterosome categories at 5dpe (Fig. 3h): Data are mean ± sem from two independent experiments. 50-100 cells were analyzed for each condition. Unpaired t test vs sh control: p=0.0008 (sh273, ***), 0.0164 (sh274, *), 0.0158 (sh277, *).

Analysis of ependymal cells categories at 15dpe (Fig. 3k): Data are mean ± sem from three independent experiments. More than 500 cells were analyzed for each condition. n= 4, 4, 3, and 3 animals for sh control, sh273, sh274 and sh277 respectively. Unpaired t test vs sh control: p= 0.0004 (sh273, ***), 0.0001 (sh274, ****), 0.0038 (sh277, **).

Mouse tracheal epithelial cells (MTECs)

MTECs cell cultures were established from the tracheas of 12 weeks old mice, according to the procedure previously published [42], with the following modification: in differentiation medium, NuSerum™ was replaced with Ultroser-G™ (Pall Corporation) and 10 µM DAPT (N-[N-(3,5-difluorophenacetyl)-L- alanyl]-S-phenylglycine t-butyl ester) (Sigma) was added one day after setting-up the air-liquid interface.

Immunostaining on HAECs and MTECs

Three days after setting-up the air-liquid interface, MTECs on Transwell membranes were pre-extracted with 0.5% Triton X-100 in PBS for 3 min, and then fixed with 4% paraformaldehyde in PBS for 15 min at room temperature. HAECs were treated 21 days after setting-up the air-liquid interface. They were fixed directly on Transwells with 100% cold methanol for 10 min at -20°C (for CDC20B and Centrin2 co-staining, Fig. S5A,B) or with 4% paraformaldehyde in PBS for 15 min at room temperature (for CDC20B single staining, Fig. S5C). All cells were then permeabilized with 0.5% Triton X-100 in PBS for 10 min and blocked with 3% BSA in PBS for 30 min. The incubation with primary and secondary antibodies was carried out at room temperature for 2 h and 1 h, respectively. Nuclei were

stained with 4,6-diamidino-2-phenylindole (DAPI). Transwell membranes were cut with a razor blade and mounted with ProLong Gold medium (Thermofisher). Primary antibodies: rabbit anti-CDC20B (1:500; Proteintech), rabbit anti-DEUP1 (1:500), anti-centrin2 (Clone 20H5, 1:500; Millipore). Secondary antibodies: Alexa Fluor 488 goat anti-rabbit (1:1000; Thermo Fisher Scientific), Alexa Fluor 647 goat anti-mouse (1:1000; Thermo Fisher Scientific). For co-staining of CDC20B and DEUP1, CDC20B was directly coupled to CF™ 594 with the Mix-n-Stain™ kit (Sigma-Aldrich) according to the manufacturer's instruction. Coupled primary antibodies were applied after secondary antibodies had been extensively washed.

Cells, transfection and western blot analysis

Cos1 cells were grown in DMEM supplemented with 10% heat inactivated FCS and transfected with Fugene HD (Roche Applied Science) according to manufacturer's protocol. Transfected or control cells were washed in PBS and lysed in 50 mM Tris-HCl pH 7.5, 150 mM NaCl, 1mM EDTA, containing 1% NP-40 and 0.25% sodium deoxycholate (modified RIPA) plus a Complete Protease Inhibitor Cocktail (Roche Applied Science) on ice. Cell extracts separated on polyacrylamide gels were transfered onto Optitran membrane (Whatman) followed by incubation with rabbit anti-CDC20B antibody (Proteintech) and horseradish peroxidase conjugated secondary antibody (Jackson Immunoresearch Laboratories). Signal obtained from enhanced chemiluminescence (Western Lightning ECL Pro, Perkin Elmer) was detected with MyECL Imager (Thermo).

Xenopus embryo injections, plasmids, RNAs, and Mos

Eggs obtained from NASCO females were fertilized *in vitro*, dejellied and cultured as described previously [43]. All injections were done at the 8-cell stage in one animal-ventral

blastomere (presumptive epidermis), except for electron microscopy analysis for which both sides of the embryo was injected, and for RT-PCR analysis for which 2-cell embryos were injected.

cdc20b riboprobe was generated from *Xenopus laevis* cDNA. Full-length sequence was subcloned in pGEM™-T Easy Vector Systems (Promega). For sense probe it was linearized by SpeI and transcribed by T7. For antisense probe it was linearized by ApaI and transcribed by Sp6 RNA polymerase. Synthetic capped mRNAs were produced with the Ambion mMESSAGE mMACHINE Kit. pCS105/mGFP-CAAX was linearized with AseI and mRNA was synthesized with Sp6 polymerase. pCS2-mRFP and pCS2-GFPgpi were linearized with NotI and mRNA was synthesized with Sp6 polymerase. pCS-centrin4-YFP (a gift from Reinhard Köster, Technische Universität Braunschweig, Germany) was linearized with NotI and mRNA was synthesized with Sp6 polymerase. pCS2-GFP-Deup1 and pCS2-Multicilin(MCI)-hGR were kindly provided by Chris Kintner and the mRNAs were obtained as described previously [9]. Embryos injected with *MCI-hGR* mRNA were cultured in Dexamethasone 20μM in MBS 0,1X from st11 until fixation. pCS2-Separase wild-type and phosphomutant 2/4 (protease dead, PD) were provided by Marc Kirchner and Olaf Stemann, respectively; plasmids were linearized with NotI and mRNAs were synthesized with Sp6 polymerase. *Venus-cdc20b*, *cdc20b-Venus* and *cdc20b* were generated by GATEWAY™ Cloning Technology (GIBCO BRL) from *Xenopus laevis cdc20b* cDNA. *cdc20b* was also subcloned in pCS2-RFP to make *RFP-cdc20b* and *cdc20b-RFP* fusions. All *cdc20b* constructs were linearized with NotI and mRNAs were synthesized with Sp6 polymerase. Quantities of mRNA injected: 0.5ng for *GFP-CAAX*, *RFP*, *GFP-GPI GFP-Deup1*, *MCI-hGR*, *Separase* and *Separase(PD)*; 1ng for *Venus-cdc20b*, *cdc20b-Venus*, *cdc20b*, *RFP-cdc20b* and *cdc20b-RFP*.

Two independent morpholino antisense oligonucleotides were designed against *cdc20b* (GeneTools, LLC). *cdc20b* ATG Mo: 5'-aaatcttctctaacttccagtccat-3', *cdc20b* Spl Mo 5'-acacatggcacaacgtacccacatc-3'. 20ng of MOs was injected per blastomere or 10ng of each Mo for co-injection.

PCR and Quantitative RT-qPCR

Xenopus embryos were snap frozen at different stages and stored at -80°C. Total RNAs were purified with a Qiagen RNeasy kit (Qiagen).

Primers were designed using Primer-BLAST Software. PCR reactions were carried out using GoTaq® G2 Flexi DNA Polymerase (Promega). RT reactions were carried out using iScript™ Reverse Transcription Supermix for RT-qPCR (BIO-RAD). qPCR reactions were carried out using SYBRGreen on a CFX Biorad qPCR cycler. To check *cdc20b* temporal expression by qPCR we directed primers to exons 9/10 junction (Forward: 5'-ggctatgaattggtgcccg-3') and exons 10/11 junction (Reverse: 5'-gcagggagcagatctggg-3') to avoid amplification from genomic DNA. The relative expression of *cdc20b* was normalized to the expression of the housekeeping gene *ornithine decarboxylase* (*ODC*) for which primers were as follows: forward: 5'-gccattgtgaagactctctccattc-3': reverse: 5'-ttcgggtgattccttgccac-3'.

To check the efficiency of Mo SPL, expected to cause retention of intron1 in the mature mRNA of *cdc20b* we directed forward (5'-cctcccgagagttagagga-3') and reverse (5'-gcatgttgtactttctgctcca-3') primers in exon1 and exon2, respectively.

To check the expression of p53 in morphants by qPCR, primers were as follows: forward: 5'-cgcagccgctatgagatgatt-3'; reverse: 5'-cacttgcggcacttaatggt-3'. The relative expression of p53 was normalized to Histone4 expression (H4) for which primers were as follows: forward: 5'-ggtgatgccctggatgttgt-3'; reverse: 5'-ggcaaaggaggaaaaggactg-3'.

Immunostainining on *Xenopus* embryos

Embryos were fixed in 4% paraformaldehyde (PFA) overnight at 4°C and stored in 100% methanol at -20°C. Embryos were rehydrated in PBT and washed in MABX (Maleic Acid Buffer + Triton X100 0,1% v/v). Next, embryos were incubated in Blocking Reagent (Roche) 2% BR + 15% Serum + MABX with respective primary and secondary antibodies (see table below). For all experiments secondary antibodies conjugated with Alexa were used. GFP-CAAX in Fig. S7E was revealed using a rabbit anti-GFP antibody together with a secondary antibody coupled to HRP, which was revealed as described previously [10]. To mark cortical actin in MCCs, embryos were fixed in 4% paraformaldehyde (PFA) in PBT (PBS + 0,1% Tween v/v) for 1h at room temperature (RT), washed 3x10 min in PBT at RT, then stained with phalloidin-Alexa Fluor 555 (Invitrogen, 1:40 in PBT) for 4 h at RT, and washed 3x10 min in PBT at RT. Primary antibodies: mouse anti-Acetylated–α-Tubulin (Clone 6-11B-1, Sigma-Aldrich, 1:1000), rabbit anti-γ-Tubulin (Abcam, 1:500), mouse anti-γ-Tubulin (Clone GTU88, Abcam, 1:500), Chicken anti-GFP (2B scientific, 1:1000), rabbit anti-GFP (Torrey Pines Biolabs, 1:500). Secondary antibodies: Alexa Fluor 647 goat anti-mouse IgG2a (1:500; Thermo Fisher Scientific), Alexa Fluor 488 goat anti-chicken (1:500; Thermo Fisher Scientific), Alexa Fluor 568 goat anti-rabbit (1:500; Thermo Fisher Scientific).

In situ hybridization on *Xenopus* embryos

Whole-mount chromogenic *in situ* hybridization was performed as described previously [43]. Whole-mount fluorescent *in situ* hybridisation (FISH) was performed as described previously [44]. For single staining, all RNA probes were labeled with digoxigenin. For FISH on section, embryos were fixed in 4% paraformaldehyde (PFA), stored in methanol for at least 4 h at −20°C, then rehydrated in PBT (PBS + Tween 0.1% v/v), treated with triethanolamine and acetic anhydride, incubated in increasing sucrose concentrations and finally embedded with

OCT (VWR Chemicals). 12µm-thick cryosections were made. Double FISH on sections was an adaptation of the whole-mount FISH method. 80ng of *cdc20b* digoxigenin-labeled sense and antisense riboprobes and 40ng of antisense *α-tubulin* fluorescein-labeled riboprobe [45] were used for hybridization. All probes were generated from linearized plasmids using RNA-labeling mix (Roche). FISH was carried out using Tyramide Signal Amplification – TSA TM Plus Cyanine 3/Fluorescein System (PerkinElmer). Antibodies: Anti-rabbit-HRP (Interchim, 1:5000), Anti-DigAP (Roche, 1:5000), Anti-DigPOD (Roche, 1:500), Anti-FluoPOD (Roche, 1:500).

Microscopy

Confocal: Flat-mounted epidermal explants were examined with a Zeiss LSM 780 confocal microscope. Four-colors confocal z-series images were acquired using sequential laser excitation, converted into single plane projection and analyzed using ImageJ software. Scanning Electron Microscopy (SEM): skin epidermis of *Xenopus* embryos from stage 37 was observed and analyzed into a digital imaging microscope (FEI TENEO). Embryos were processed as described previously [44]. Transmission Electron Microscopy (TEM): St25 embryos were fixed overnight at 4°C in 2.5% glutaraldehyde, 2% paraformaldehyde, 0.1% tannic acid in a sodium cacodylate buffer 0.05 M pH7.3. Next, embryos were washed 3x15 min in cacodylate 0.05 M at 4°C. Post-fixation was done in 1% osmium buffer for 2 h. Next, embryos were washed in buffer for 15 min. Then, embryos were washed in water and dehydrated conventionally with alcohol, followed by a step in 70% alcohol containing 2% uranyl during 1 to 2 h at RT, or overnight at 4°C. After 3 times in 100% alcohol, completed with 3 washes of acetone. Next, embryos were included in classical epon resin, which was polymerized in oven at 60°C for 48 h. Sections of 80 nm were made and analyzed into an FMI TECNAI microscope with acceleration of 200kV.

Statistical analysis of *Xenopus* experiments

To quantify the effect of our different experiments, we applied One-way ANOVA analysis and Bonferroni's multiple comparisons test (t test). ***P<0.05; ns = not significant. Statistical analyses were done using GraphPad Prism 6.

Fig. 3J: 10 cells per condition were analyzed and the total number of γ-tubulin positive spots per injected cell was counted.

Fig. 4N: 5 fields (20x zoom) per condition were analyzed, and the total number of properly ciliated MCCs based on acetylated α-tubulin staining among GFP positive cells per field was counted. Each field corresponded to a different embryo.

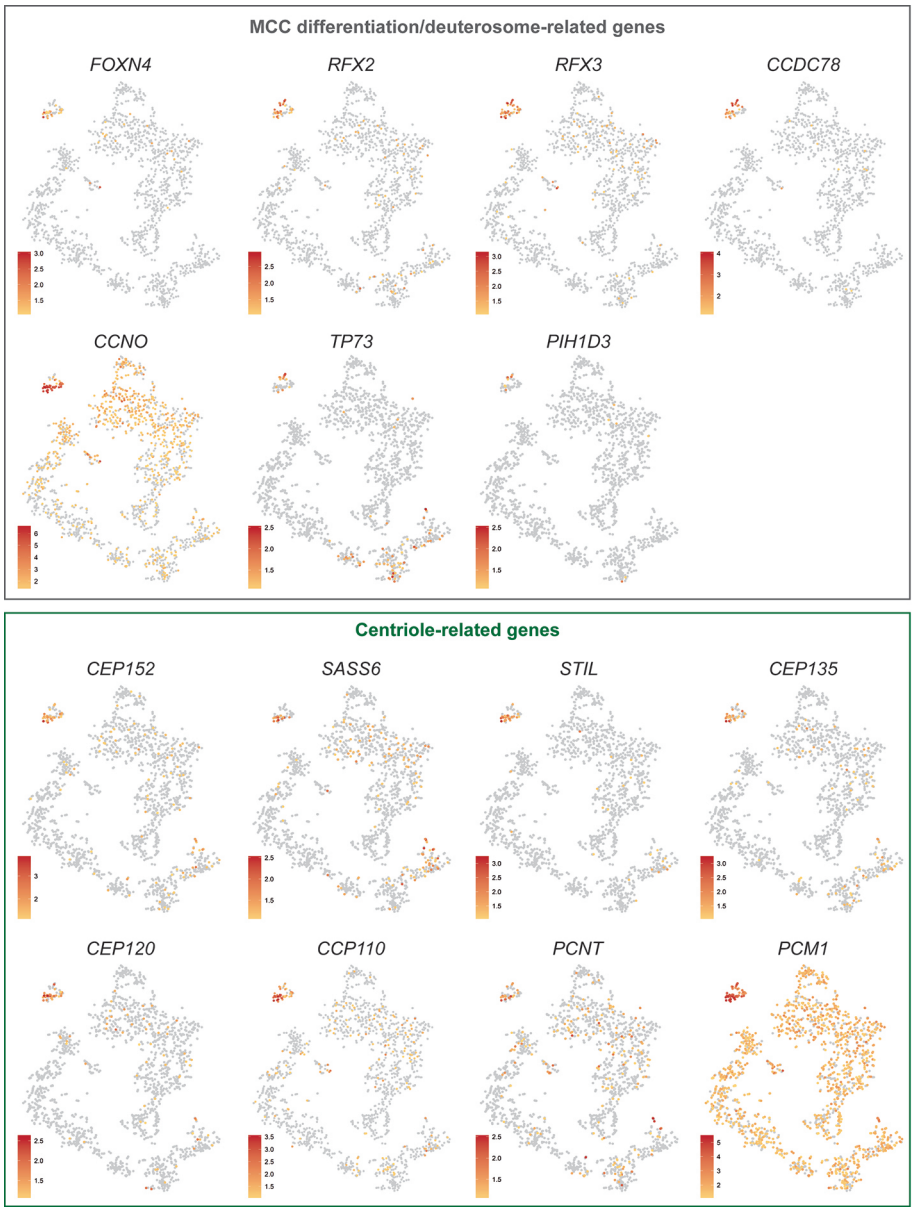

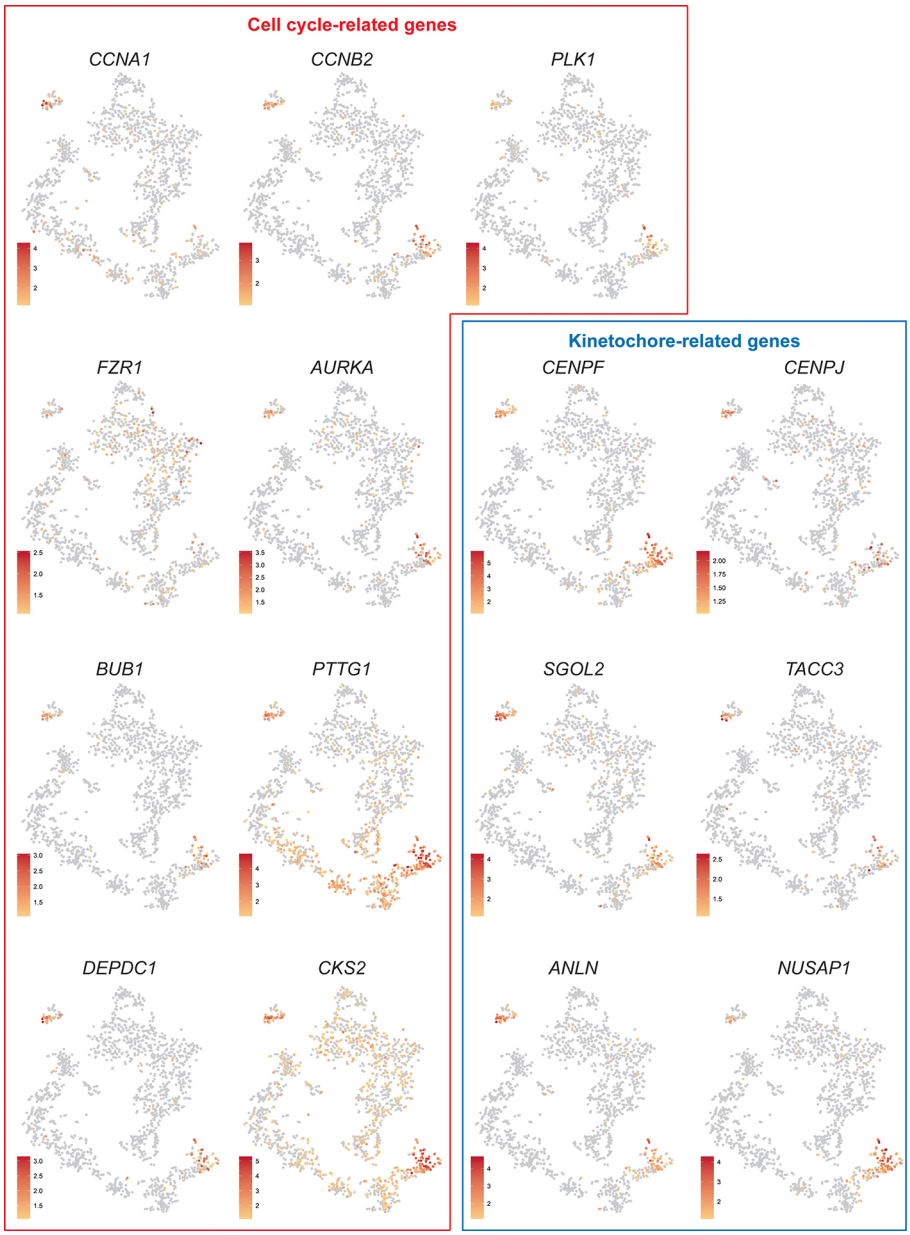

Figure S1: Single cell RNA-seq analysis of HAECs.

tSNE plots for a selection of genes expressed at the single-cell level, in deuterosomal-stage differentiating HAECs. Genes were grouped into functional categories.

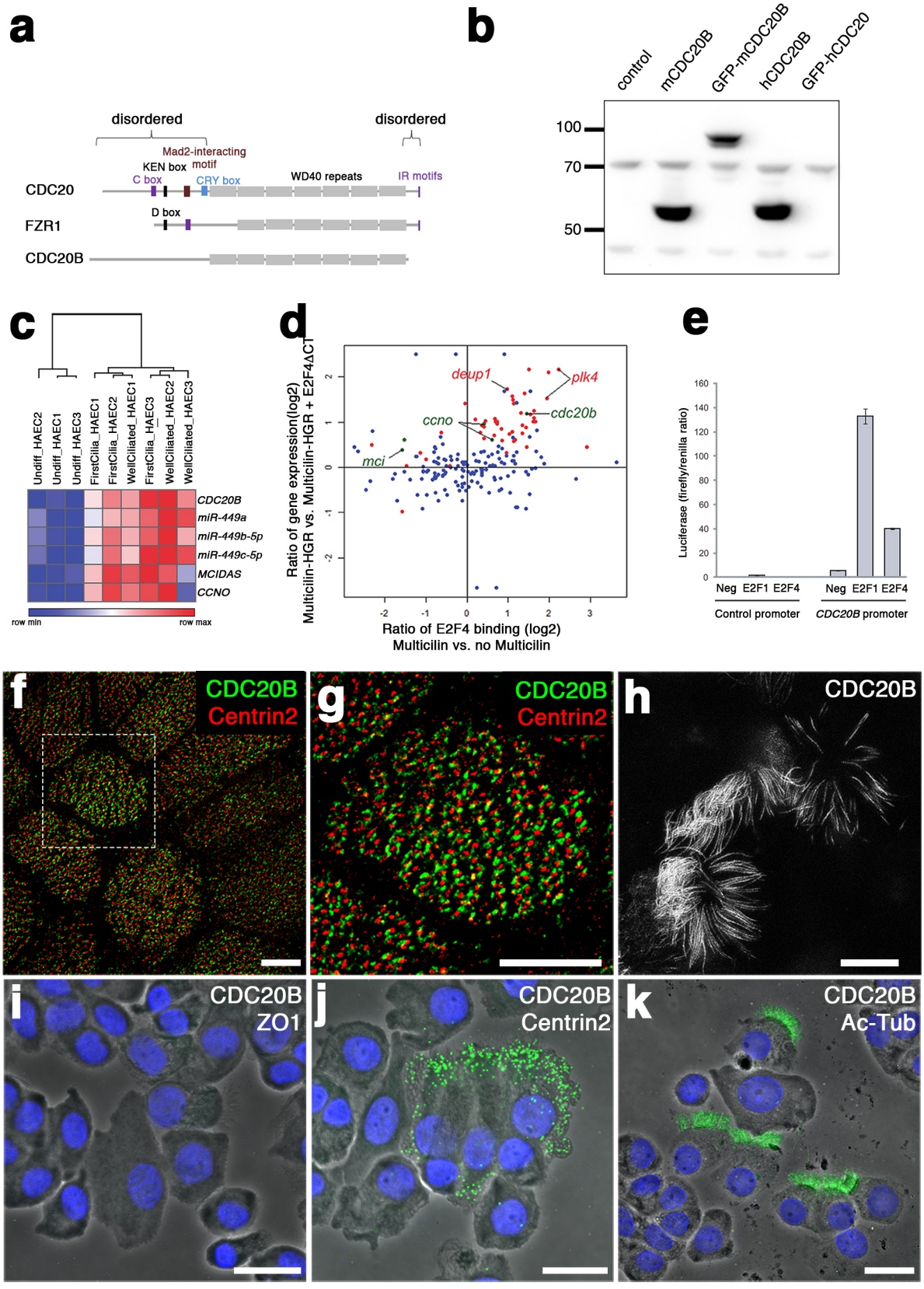

Figure S2: Structure, regulation and sub-cellular localization of CDC20B.

(a) Domain composition of CDC20 family members. The C box and IR motifs in CDC20 and FZR1 serve as APC/C binding domains. The KEN box and the Cry box in CDC20, and the D box in FZR1 are involved in their regulation by degradation. The Mad2-interacting motif in CDC20 is important for its regulation by the spindle assembly checkpoint. WD40 repeats are involved in substrate recognition. Note that CDC20B lacks degradation motifs and the APC/C binding domains present in CDC20 and FZR1. (**b**) COS1 cells were transfected with vectors coding for indicated proteins and immunoblot was performed using Proteintech rabbit anti-CDC20B antibody. This antibody recognized mouse and human CDC20B but did not cross-react with human CDC20. (**c-e**). ***CDC20B* is induced during multiciliogenesis under the control of E2Fs/MCIDAS. (c)** Heatmap of gene expression measured by RNA-seq or small RNA-seq on 3 independent HAEC differentiation time courses (HAEC1 to HAEC3). Normalized read counts were Log2-transformed and median-centered by gene. Hierarchical clustering (Euclidian distance) was performed on samples. The scale color bar indicates the minimum and maximum values per row. (**d**) Promoter luciferase reporter assay. Promoter-associated firefly luciferase was normalized by constitutive renilla luciferase. Control and *CDC20B* promoter were co-expressed with a plasmid expressing E2F1 or E2F4, or a negative control. Bars represent the average of 3 independent experiments. Error bars represent the standard deviation. (**e**) Ratio of gene expression (Multicilin-HGR vs. Multicilin-HGR +E2F4ΔCT) vs. ratio of E2F4 binding (Multicilin vs. no Multicilin). E2F4ΔCT prevents the formation of transcriptionally active Multicilin/E2F complexes. Centriole-related genes are highlighted in red. Genes from the multiciliary locus are highlighted in green. Data was obtained by mapping and quantifying raw data from[13]. (**f-k**) **CDC20B sub-cellular localization in human mature MCCs. (f,g)** ALI day 21 HAECs were fixed in methanol, and immunostained against CDC20B and Centrin2. STED super-resolution microscopy revealed the association of CDC20B to BBs. (**h**) ALI day 21 HAECs were fixed in paraformaldehyde,

and immunostained against CDC20B. STED super-resolution microscopy revealed the association of CDC20B with cilia. (**i-k**) DuoLink Assays on fully differentiated HAECs after cytospin. (**i**) Assay with CDC20B and ZO-1 antibodies was used as negative control. (**j**) Assay with CDC20B and Centrin2 (BBs) antibodies. (**k**) Assay with CDC20B and Acetylated-α-Tubulin (cilia) antibodies. Interaction between antibodies separated by less than 40nm generated green fluorescent signal. Nuclei are stained in blue. Scale bar= 5μm (**f-h**); 20μm (**i-k**).

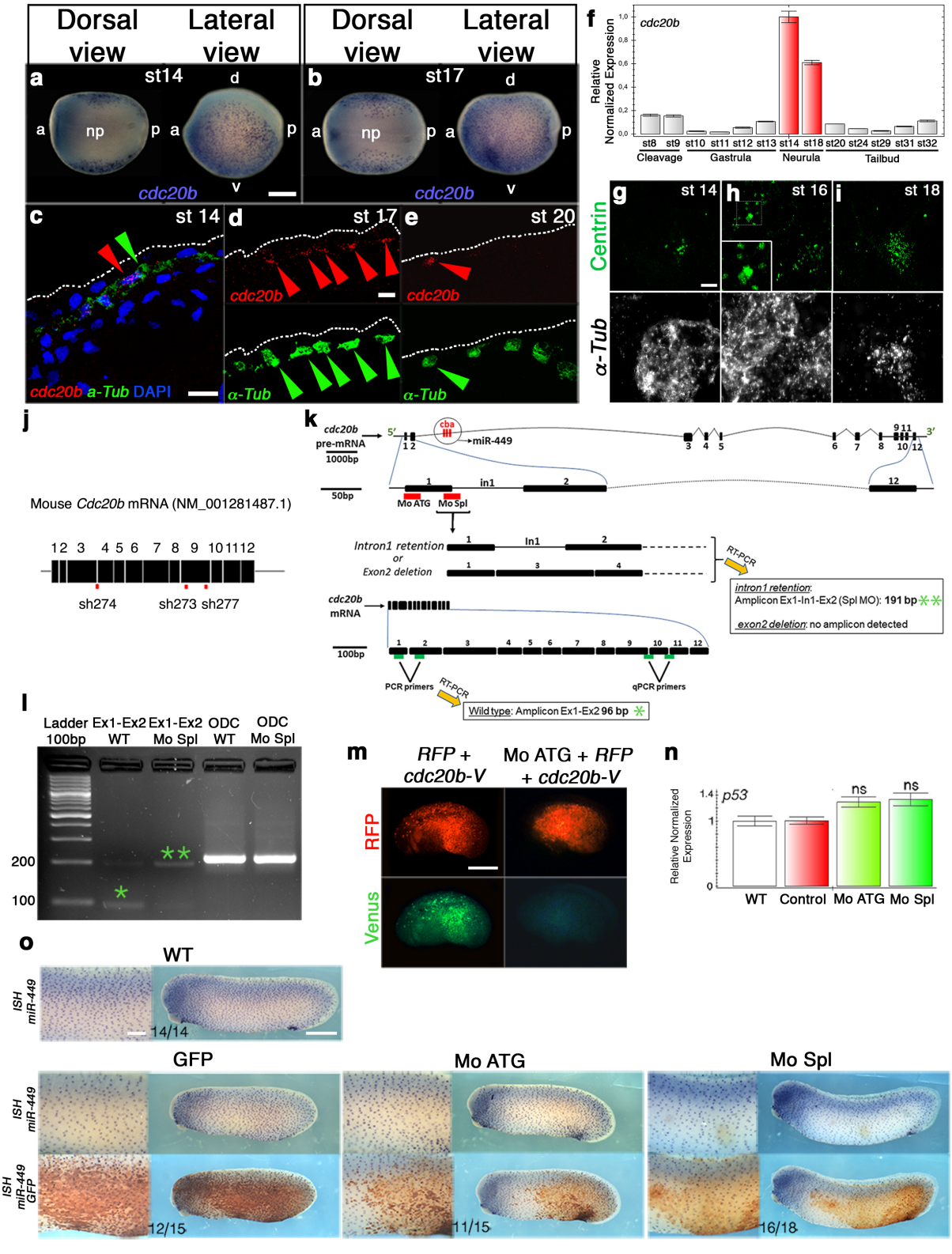

Figure S3: *cdc20b* expression and knockdown in *Xenopus*.

(**a**,**b**) *cdc20b* whole-mount *in situ* hybridization in early neurula st14 and st17, respectively. *cdc20b* mRNA is expressed in epidermal cells but not in the neural plate (np), as revealed on dorsal views. a: anterior, p: posterior, d: dorsal, v: ventral. (**c-e**) *cdc20b* (red) and *α-Tubulin* (α-*Tub,* green) double fluorescent *in situ* hybridization (FISH) on sectioned embryos at st14 (**c**), st17 (**d**) and st20 (**e**). Red and green arrows point immature MCCs co-expressing *cdc20b* and *α-Tub*. Nuclei are revealed by DAPI staining in blue. White dotted lines indicate the surface of the epidermis. Note that the majority of MCCs become negative for *cdc20b* expression at st20. (**f**) RT-qPCR showing the relative expression of *cdc20b* from st8 (mid-blastula transition) until tadpole st32 normalized with *ODC* expression. Red bars indicate the peak of *cdc20b* transcript accumulation between st14 and st18, when centriole amplification occurs. (**g-i**) To reveal the dynamics of centriole multiplication, MCCs were stained by α-*Tub* FISH and by immunostaining against Centrin. Multiple Centrin-positive foci were detected at st14, marking the onset of centriologenesis. Procentriole aggregates, presumably organized around deuterosomes were clearly visualized at st16 (inset). Dispersed multiple centrioles were detected at st18. (**j-o**) **Description and validation of knockdown strategies**. (**j**) Schematic representation of mouse *Cdc20b* mRNA and position of shRNAs used in this study. Note that sh274 targeted the junction between exons 3 and 4, ruling out possible interference with the production of miR-449 molecules from the *Cdc20b* pre-mRNA. (**k**) Schematic representation of *Xenopus cdc20b* pre-mRNA with introns, exons and miR-449abc relative position and size. Red horizontal bars below exon1 show the position of *cdc20b* Mo ATG and Mo Spl. On the bottom, green horizontal bars indicate RT-PCR and qPCR primer position. (**l**) RT-PCR confirmed that Mo Spl caused intron1 retention (amplicon=191bp; double green stars), which is expected to introduce a premature stop codon and to produce a Cdc20b protein lacking 96% of its amino-acids, likely to undergo unfolded protein response-mediated degradation. (**m**) The efficiency of Mo ATG was verified through fluorescence extinction of

co-injected Cdc20b-Venus. (**n**) RTqPCR revealed that neither *cdc20b* morpholinos caused significant *p53* transcript up-regulation, a non-specific response sometimes detected in zebrafish embryos subjected to morpholinos. Four independent experiments were carried out to check *p53* expression in morphant conditions. (**o**) miR-449 expression revealed by whole-mount *in situ* hybridization with LNA probes was not perturbed in the presence of either morpholinos. Embryos were photographed before (top) and after (bottom) staining against co-injected GFP-CAAX to be able to detect miR-449 staining. The number of embryos showing normal miR-449 expression over the total number of embryos analyzed is indicated on the photographs. Scale bars: 250µm (**a**), 20µm (**c**,**d**); 5µm (**g**); 500µm (**m**); 500µm (**o**, whole embryo); 80µm (**o**, zoom).

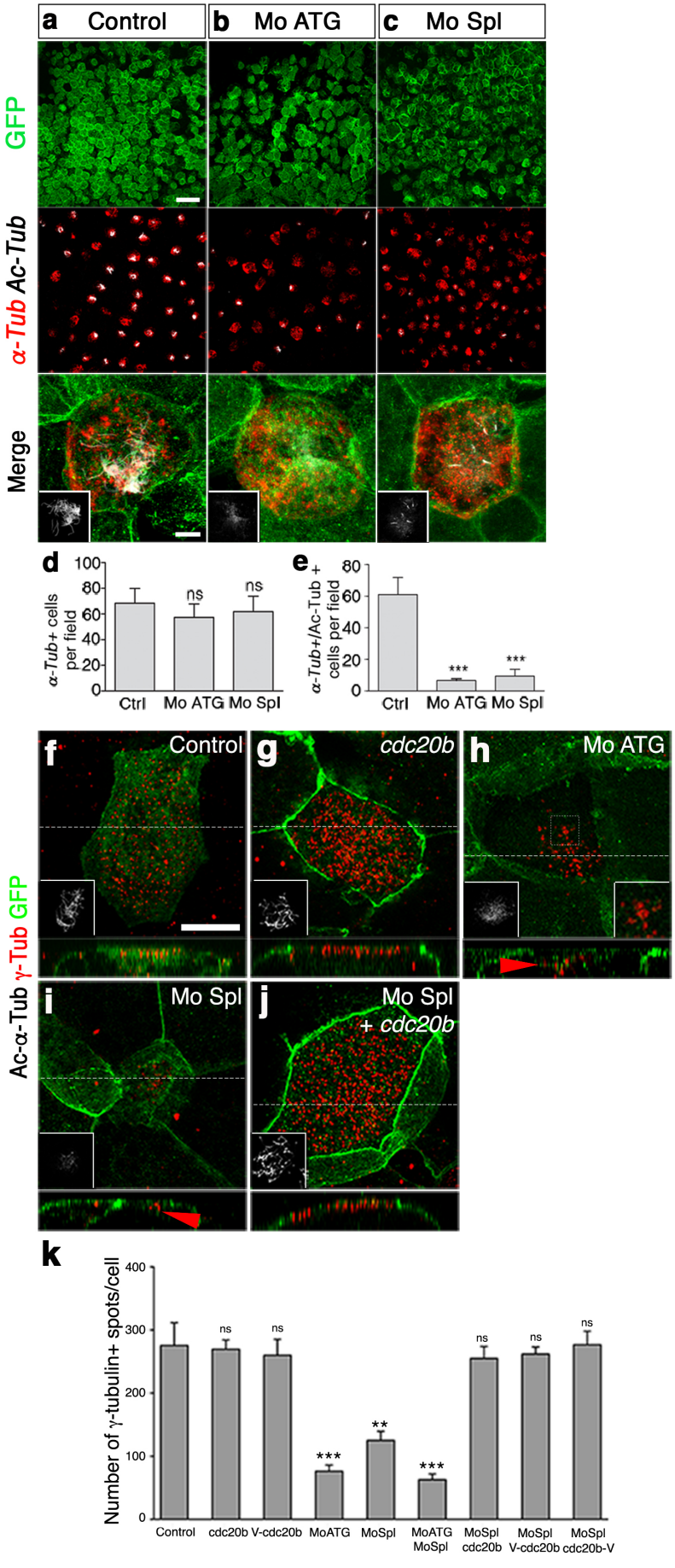

Figure S4: *cdc20b* knockdown impairs multiciliogenesis in *Xenopus*.

(**a-e**) 8-cell embryos were injected in presumptive epidermis with *cdc20b* morpholinos and *GFP-caax* mRNA (injection tracer) as indicated. Control was provided by *GPF-caax* injection alone. Embryos at tailbud st25 were processed for fluorescent staining against GFP (green), Acetylated α-Tubulin (cilia, white) and *α-Tub* mRNA (MCC marker, red). Insets show cilia staining. Note that *cdc20b* morphant MCCs maintain expression of fate marker *α-Tub* but poorly grow cilia. (**d**) Bar graph showing quantification of *α-Tub*/GFP positive cells. (**e**) Bar graph showing quantification of *α-Tub*/Ac-Tub/GFP positive cells. 10 fields corresponding to 10 different embryos were analyzed for each condition. (**f-k**) ***cdc20b* knockdown impairs the formation of centrioles and cilia.** Embryos were injected as in **a-c**, and immunostained at tailbud st25 against GFP (injection tracer, green), γ-tubulin (BBs, red) and Acetylated α-Tubulin (cilia, white, left insets). Right inset in **h**: zoom on a stalled deuterosomal figure. z-projections made along white dotted lines are shown in bottom panels. Arrowheads point undocked BBs. (k) Bar graph showing the quantification of γ-tubulin spots per MCC. Note that BB numbers were restored to normal levels in *cdc20b* Spl morphants by tagged and untagged versions of *cdc20b*. Scale bars: 50µm (**a**), 5µm (zoom in **a**, bottom); 5µm (**f**).

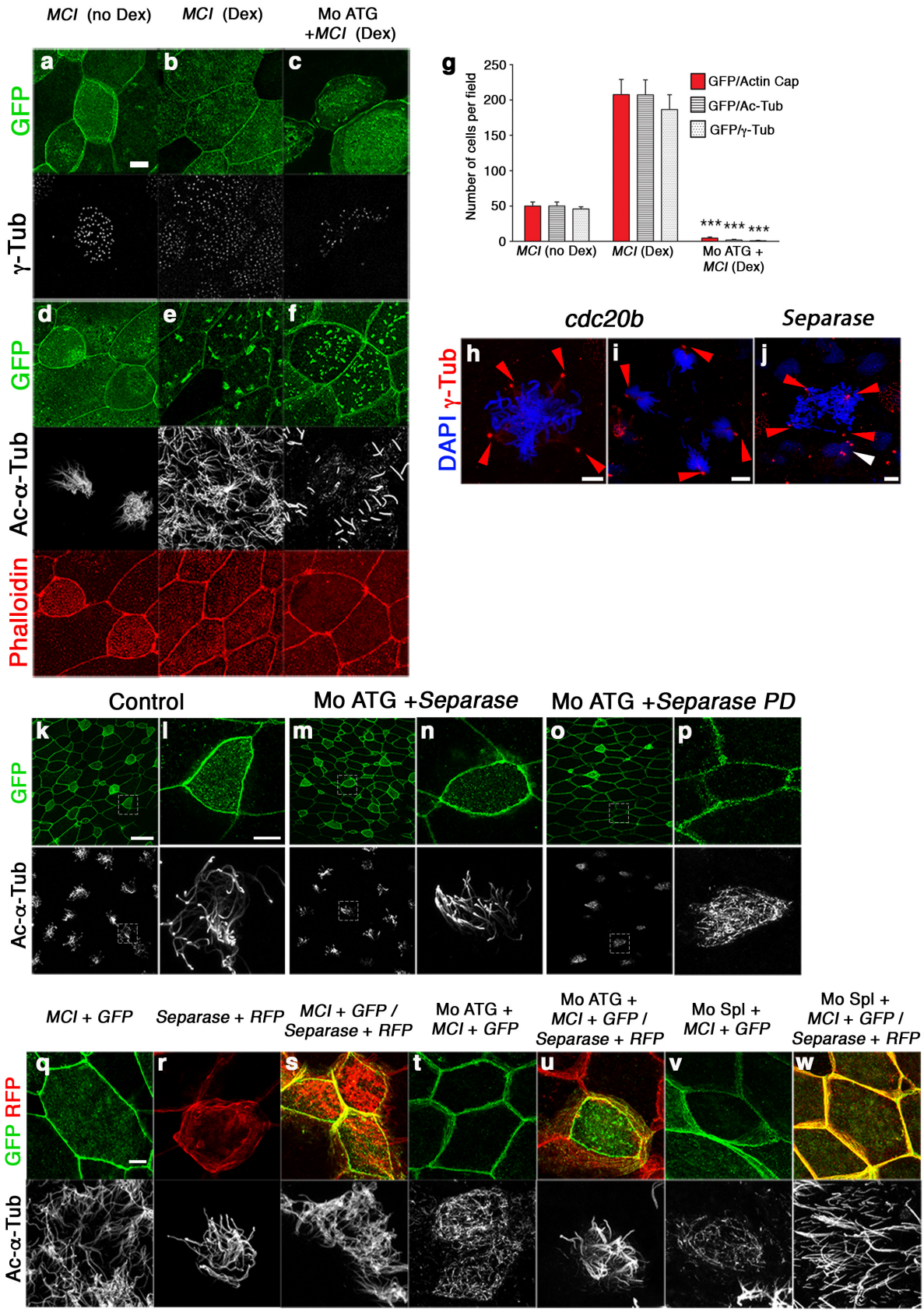

Figure S5: *cdc20b* knockdown prevents multiciliogenesis induced by Multicilin, and is

counteracted by Separase overexpression.

(**a-g**) ***cdc20b* knockdown prevents multiciliogenesis induced by Multicilin.** 8-cell embryos were injected in presumptive epidermis with *Multicilin-hGR* mRNA (*MCI*) and *cdc20b* Mo ATG, as indicated. *GFP-GPI* mRNA was co-injected as a tracer. MCI-hGR-injected embryos were induced with dexamethasone at st11. To check the efficiency of MCI induction some embryos were not treated with dexamethasone and served as controls (no DEX). Embryos were fixed at tailbud st25, and were stained against GFP (green) and γ-Tubulin (basal bodies, white)(**a-c**), or against GFP (green) phalloidin (apical actin, red), and Acetylated-α-Tubulin (cilia, white)(**d-f**). Note that *cdc20b* morphant MCI-induced MCCs failed to amplify centrioles, to maintain a proper actin cap, and to grow cilia. (**g**) Bar graph showing the quantification of GFP-positive cells that displayed normal actin, basal body and cilium staining. 5 fields (40x) per condition were analyzed. (**h-j**) **Cdc20b and Separase overexpression induces multipolar spindles in non-MCCs.** 8-cell embryos were injected in presumptive epidermis with *Xenopus Venus-cdc20b* (**h**,**i**) and human *Separase* mRNAs (**j**). Immunofluorescence against ɣ-Tub (centrosome, red) and DAPI staining (nuclei, blue) was performed at tailbud st25. Red arrowheads indicate multiple centrosomes in non-MCC dividing cells (**h**: metaphase; **i**: telophase, **j**: anaphase). The formation of multipolar mitotic spindles was consistent with Cdc20b and Separase forcing centriole separation. The white arrowhead indicates excess centrosomes in a non-MCC interphasic cell. (**k-w**) **Wild-type but not protease-dead Separase rescues multiciliogenesis in MCCs deficient for Cdc20b.** (**k-p**) 8-cell embryos were injected in presumptive epidermis with *GFP-GPI* mRNA, human *Separase* mRNA, and *cdc20b* Mo ATG, as indicated. Immunofluorescence against GFP (injection tracer, green), and Acetylated-α-Tubulin (cilia, white) was performed at tailbud st25. Cells in dotted squares were blown up for better visualization. Note that multiciliogenesis was rescued in *cdc20b* morphant MCCs by wild-type (**m**,**n**) but not

protease-dead Separase (**o**,**p**). (**q**-**w**) 4-cell embryos were injected in one ventral blastomere (presumptive epidermis) with *MCI-hGR* and *GFP-GPI* mRNAs, in the presence or not of *cdc20b* morpholinos, as indicated. Next, at 16-cell stage, half of those embryos were injected with human *Separase* and RFP mRNAs in one ventral-animal blastomere. This setup was designed to avoid co-injection of *cdc20b* morpholinos with *Separase* mRNA, ruling out non-specific interference *in vitro* between these reagents. MCI-hGR-injected embryos were induced with dexamethasone at st11. All embryos were fixed at tailbud st25 and stained for GFP (*cdc20b* Mo tracer, green), RFP (*Separase* tracer, red) and Acetylated-α-Tubulin (cilia, white). Note that multiciliogenesis failed in MCI-induced *cdc20b* morphant MCCs (**t,v).** The presence of Separase rescued multiciliogenesis in MCI-induced *cdc20b* morphant MCCs (**u**,**w**). Scale bars: 5µm (**a**,**h**,**i**,**j**,**l**,**q**); 20µm (**k**).

G1/S	
Symbol	Ensembl
ORC1	ENSG00000085840
ZNF367	ENSG00000165244
ADAMTS1	ENSG00000154734
CCNE2	ENSG00000175305
CDC25A	ENSG00000164045
RECQL4	ENSG00000160957
DTL	ENSG00000143476
CDC6	ENSG00000094804
CCNE1	ENSG00000105173
MCM2	ENSG00000073111
GINS3	ENSG00000181938
CHAF1B	ENSG00000159259
WDR76	ENSG00000092470
MCM6	ENSG00000076003
CLSPN	ENSG00000092853
CDCA7	ENSG00000144354
OSBPL6	ENSG00000079156
RAB23	ENSG00000112210
PLCXD1	ENSG00000182378
SKP2	ENSG00000145604
MDM1	ENSG00000111554
GINS2	ENSG00000131153
E2F1	ENSG00000101412
MCM5	ENSG00000100297
SNHG10	ENSG00000247092
HSF2	ENSG00000025156
UBR7	ENSG00000012963
RMI2	ENSG00000175643
NUP43	ENSG00000120253
ACD	ENSG00000102977
ZMYND19	ENSG00000165724
MSH2	ENSG00000095002
CDCA7L	ENSG00000164649
KIAA1586	ENSG00000168116
PMS1	ENSG00000064933
UNG	ENSG00000076248
KIAA1147	ENSG00000257093
POLD3	ENSG00000077514
ANKRD10	ENSG00000088448
CHAF1A	ENSG00000167670
BARD1	ENSG00000138376
INTS8	ENSG00000164941
APEX2	ENSG00000169188
ACYP1	ENSG00000119640
MRI1	ENSG00000037757
INSR	ENSG00000171105
TOPBP1	ENSG00000163781
FAM105B	ENSG00000154124
NPAT	ENSG00000149308
PCDH7	ENSG00000169851
GMNN	ENSG00000112312
RNPC3	ENSG00000185946
RNF113A	ENSG00000125352
FAM122A	ENSG00000187866
CAPN7	ENSG00000131375
TIPIN	ENSG00000075131
C14orf142	ENSG00000170270
LNPEP	ENSG00000113441
USP53	ENSG00000145390
PANK2	ENSG00000125779
VPS72	ENSG00000163159
DIS3	ENSG00000083520

S	
Symbol	Ensembl
ANKRD18A	ENSG00000273170
REEP1	ENSG00000068615
DEPDC7	ENSG00000121690
CDC7	ENSG00000097046
DNA2	ENSG00000138346
EXO1	ENSG00000174371
KDELC1	ENSG00000134901
ANKRD18A	ENSG00000180071
BRIP1	ENSG00000136492
PKMYT1	ENSG00000127564
CDC45	ENSG00000093009
C11orf82	ENSG00000165490
BLM	ENSG00000197299
RAD51	ENSG00000051180
CCDC150	ENSG00000144395
CDCA5	ENSG00000146670
CPNE8	ENSG00000139117
MCM8	ENSG00000125885
ESCO2	ENSG00000171320
GOLGA8B	ENSG00000215252
ASF1B	ENSG00000105011
FANCA	ENSG00000187741
INTS7	ENSG00000143493
POLA1	ENSG00000101868
FANCI	ENSG00000140525
RRM2	ENSG00000171848
TTLL7	ENSG00000137941
RAD51AP1	ENSG00000111247
KAT2B	ENSG00000114166
CHML	ENSG00000203668
BRCA1	ENSG00000012048
ABHD10	ENSG00000144827
TYMS	ENSG00000176890
PRIM1	ENSG00000198056
TTC31	ENSG00000115282
E2F8	ENSG00000129173
CENPQ	ENSG00000031691
PHTF1	ENSG00000116793
MASTL	ENSG00000120539
OSGIN2	ENSG00000164823
GOLGA8A	ENSG00000175265
PHTF2	ENSG00000006576
BBS2	ENSG00000125124
BMI1	ENSG00000168283
FEN1	ENSG00000168496
RMI1	ENSG00000178966
NSUN3	ENSG00000178694
KAT2A	ENSG00000108773
CENPM	ENSG00000100162
ZWINT	ENSG00000122952
ORC3	ENSG00000135336
KIAA1598	ENSG00000187164
BIVM	ENSG00000134897
DNAJB4	ENSG00000162616
CCDC84	ENSG00000186166
DCAF16	ENSG00000163257
NUP160	ENSG00000030066
RFC2	ENSG00000049541
CDKN2AIP	ENSG00000168564
UBE2T	ENSG00000077152
DHFR	ENSG00000228716
PTAR1	ENSG00000188647
RAD18	ENSG00000070950
OGT	ENSG00000147162
EZH2	ENSG00000106462
C5orf42	ENSG00000197603
LYRM7	ENSG00000186687
CCDC14	ENSG00000175455
NAB1	ENSG00000138386
SP1	ENSG00000185591
RPA2	ENSG00000117748
RBBP8	ENSG00000101773
RRM1	ENSG00000167325
FAM178A	ENSG00000119906
SAP30BP	ENSG00000161526
NT5DC1	ENSG00000178425
CERS6	ENSG00000172292
ZBED5	ENSG00000236287
MAP3K2	ENSG00000169967

G2/M	
Symbol	Ensembl
IQGAP3	ENSG00000183856
TRAIP	ENSG00000183763
CDC25C	ENSG00000158402
NEIL3	ENSG00000109674
PIF1	ENSG00000140451
KIFC1	ENSG00000237649
HJURP	ENSG00000123485
NCAPH	ENSG00000121152
KIF23	ENSG00000137807
SKA3	ENSG00000165480
KIAA1524	ENSG00000163507
NDC80	ENSG00000080986
CCNF	ENSG00000162063
CDCA8	ENSG00000134690
PSRC1	ENSG00000134222
FANCD2	ENSG00000144554
ESPL1	ENSG00000135476
CDR2	ENSG00000140743
AURKB	ENSG00000178999
BORA	ENSG00000136122
LMNB1	ENSG00000113368
TRIM59	ENSG00000213186
CHEK2	ENSG00000183765
MND1	ENSG00000121211
CDCA2	ENSG00000184661
CKAP2L	ENSG00000169607
STIL	ENSG00000123473
POLQ	ENSG00000051341
MELK	ENSG00000165304
CENPL	ENSG00000120334
LIX1L	ENSG00000152022
KIF11	ENSG00000138160
C14orf80	ENSG00000185347
UBE2C	ENSG00000175063
NCAPD3	ENSG00000151503
HAUS8	ENSG00000131351
FAM83D	ENSG00000101447
CDK1	ENSG00000170312
MAD2L1	ENSG00000164109
GABPB1	ENSG00000104064
SAP30	ENSG00000164105
CFD	ENSG00000197766
TTF2	ENSG00000116830
MID1	ENSG00000101871
GAS1	ENSG00000180447
TUBA1A	ENSG00000167552
ZNF587	ENSG00000198466
TUBD1	ENSG00000108423
FAN1	ENSG00000198690
CDKN2C	ENSG00000123080
TUBB2A	ENSG00000137267
TNPO2	ENSG00000105576
ZNHIT2	ENSG00000174276
TRMT2A	ENSG00000099899
PKNOX1	ENSG00000160199
ENTPD5	ENSG00000187097
KDM4A	ENSG00000066135
STK17B	ENSG00000081320
KLF6	ENSG00000067082
KATNA1	ENSG00000186625
H2AFX	ENSG00000188486
BRD8	ENSG00000112983
RCCD1	ENSG00000166965
CDKN1B	ENSG00000111276
UACA	ENSG00000137831
KCTD9	ENSG00000104756
ATL2	ENSG00000119787
KPNA2	ENSG00000182481
HRSP12	ENSG00000132541
VTA1	ENSG00000009844
HMGB2	ENSG00000164104
C2orf69	ENSG00000178074
FADD	ENSG00000168040
HIPK2	ENSG00000164393
KIF22	ENSG00000079616
MGAT2	ENSG00000168282
NR3C1	ENSG00000113580
DHX8	ENSG00000067596
NMB	ENSG00000197696
TFAP2A	ENSG00000137203
HINT3	ENSG00000111911
CDC16	ENSG00000130177
NUMA1	ENSG00000137497
ARMC1	ENSG00000104442
STAT1	ENSG00000115415
CCDC107	ENSG00000159884
TMPO	ENSG00000120802

M	
Symbol	Ensembl
CKS1B	ENSG00000268942
DEPDC1B	ENSG00000035499
SHCBP1	ENSG00000171241
FAM64A	ENSG00000129195
FYN	ENSG00000010810
KIF2C	ENSG00000142945
SPAG5	ENSG00000076382
CIT	ENSG00000122966
CENPA	ENSG00000115163
DIAPH3	ENSG00000139734
CADM1	ENSG00000182985
KIF14	ENSG00000118193
PLK1	ENSG00000166851
MDC1	ENSG00000137337
DEPDC1	ENSG00000024526
BUB1	ENSG00000169679
DLGAP5	ENSG00000126787
NUF2	ENSG00000143228
CEP55	ENSG00000138180
GTSE1	ENSG00000075218
HMMR	ENSG00000072571
FOXM1	ENSG00000111206
E2F5	ENSG00000133740
PRR11	ENSG00000068489
NEK2	ENSG00000117650
TACC3	ENSG00000013810
CENPE	ENSG00000138778
CCNB2	ENSG00000157456
CDC20	ENSG00000117399
BIRC5	ENSG00000089685
CCDC88A	ENSG00000115355
POC1A	ENSG00000164087
MKI67	ENSG00000148773
MKI67	ENSG00000148773
HSPA13	ENSG00000155304
CDC25B	ENSG00000101224
TPX2	ENSG00000088325
AURKA	ENSG00000087586
ANKRD40	ENSG00000154945
CENPF	ENSG00000117724
CNTROB	ENSG00000170037
NCAPD2	ENSG00000010292
SGOL2	ENSG00000163535
SRF	ENSG00000112658
DZIP3	ENSG00000198919
ECT2	ENSG00000114346
ORAOV1	ENSG00000149716
NUP35	ENSG00000163002
PTPN9	ENSG00000169410
HS2ST1	ENSG00000153936
RCAN1	ENSG00000159200
SS18	ENSG00000141380
HCFC1	ENSG00000172534
NUP98	ENSG00000110713
POM121	ENSG00000196313
TOMM34	ENSG00000025772
CKAP5	ENSG00000175216
GRK6	ENSG00000198055
SEPHS1	ENSG00000086475
QRICH1	ENSG00000198218
AHI1	ENSG00000135541
CNOT10	ENSG00000182973
KLF9	ENSG00000119138
SETD8	ENSG00000183955
ATF7IP	ENSG00000171681
RAD51C	ENSG00000108384
CDC42EP1	ENSG00000128283
HPS4	ENSG00000100099
GOT1	ENSG00000120053
MZT1	ENSG00000204899
RRP1	ENSG00000160214
AKIRIN2	ENSG00000135334
CDC27	ENSG00000004897
SMARCD1	ENSG00000066117
BIRC2	ENSG00000110330

M/G1	
Symbol	Ensembl
TROAP	ENSG00000135451
CDKN3	ENSG00000100526
PRC1	ENSG00000198901
HSD17B11	ENSG00000198189
BTBD3	ENSG00000132640
SLC39A10	ENSG00000196950
GTF3C4	ENSG00000125484
WWC1	ENSG00000113645
ELP3	ENSG00000134014
FOXK2	ENSG00000141568
OPN3	ENSG00000054277
KIAA0586	ENSG00000100578
ANTXR1	ENSG00000169604
CEP70	ENSG00000114107
HMGCR	ENSG00000113161
TULP4	ENSG00000130338
ZNF281	ENSG00000162702
CDK7	ENSG00000134058
LYAR	ENSG00000145220
PPP6R3	ENSG00000110075
DCP1A	ENSG00000162290
FAM189B	ENSG00000160767
AGPAT3	ENSG00000160216
PSEN1	ENSG00000080815
NUP37	ENSG00000075188
MSL1	ENSG00000188895
AGFG1	ENSG00000173744
SNUPN	ENSG00000169371
STAG1	ENSG00000118007
LRIF1	ENSG00000121931
PAK1IP1	ENSG00000111845
NCOA3	ENSG00000124151
PTTG1	ENSG00000164611
CTR9	ENSG00000198730
DKC1	ENSG00000130826
FOPNL	ENSG00000133393
VCL	ENSG00000035403
MRPS2	ENSG00000122140
WIPF2	ENSG00000171475

Table S1. Gene sets used to determine the position in the cell cycle of individual cells analyzed by scRNA-seq.